Constraining Type II 2HDM in Light of LHC Higgs Searches

Baradhwaj Coleppa, Felix Kling, Shufang Su*

Department of Physics, University of Arizona, Tucson, AZ 85721, USA

Abstract

We study the implication of the LHC Higgs search results on the Type II Two Higgs-Doublet Model. In particular, we explore the scenarios in which the observed 126 GeV Higgs signal is interpreted as either the light CP-even Higgs h^0 or the heavy CP-even Higgs H^0. Imposing both theoretical and experimental constraints, we analyze the surviving parameter regions in m_H (m_h), m_A, $m_{H^\pm}$, $\tan\beta$ and $\sin(\beta-\alpha)$. We further identify the regions that could accommodate a 126 GeV Higgs with cross sections consistent with the observed Higgs signal. We find that in the h^0-126 case, we are restricted to narrow regions of $\sin(\beta-\alpha)\sim\pm1$ with $\tan\beta$ up to 4, or extended regions in $\sin(\beta-\alpha)$ with $\tan\beta<1$. The values of m_H, m_A and $m_{H^\pm}$, however, are relatively unconstrained. In the H^0-126 case, we are restricted to a narrow region of $\sin(\beta-\alpha)\sim0$ with $\tan\beta$ up to about 7, or an extended region of $\sin(\beta-\alpha)$ between -0.6 to -0.1, with $\tan\beta$ extended to 30 or higher. m_A and $m_{H^\pm}$ are nearly degenerate due to $\Delta\rho$ constraints. Imposing flavor constraints shrinks the surviving parameter space significantly. We also investigate the correlation between $\gamma\gamma$, VV and $bb/\tau\tau$ channels. $\gamma\gamma$ and VV channels are most likely to be highly correlated with $\gamma\gamma:VV\sim1$ for the normalized cross sections.

*Electronic address: baradhwa@email.arizona.edu, kling@email.arizona.edu,shufang@physics.arizona.edu

I. INTRODUCTION

The discovery of a resonance at 126 GeV with properties consistent with the Standard Model (SM) Higgs boson in both the ATLAS [1, 2] and CMS experiments [3, 4] is undoubtedly the most significant experimental triumph of the Large Hadron Collider (LHC) to date. The nature of this particle, as regards its CP properties and couplings, are currently being established [4, 5]. Though further data would undoubtedly point us in the right direction, at this point it is useful to explore the implication of the current Higgs search results on models beyond the SM. There are quite a few models that admit a scalar particle in their spectrum and many of them can have couplings and decays consistent with the SM Higgs boson. Thus it behooves us to constrain these models as much as possible with the Higgs search results at hand.

One of the simplest extensions of the SM involves enlarged Higgs sectors. This can be done by simply adding more scalar doublets, or considering Higgs sectors with more complicated representations. In the work, we will study the Two Higgs-Doublet Models (2HDM) that involves two scalar doublets both charged under the SM $\mathrm{SU}(2)_L \times \mathrm{U}(1)_Y$ gauge symmetries [6–9]. The neutral components of both the Higgs fields develop vacuum expectation values (vev), breaking $\mathrm{SU}(2)_L \times \mathrm{U}(1)_Y$ down to $\mathrm{U}(1)_{\mathrm{em}}$. Assuming no CP-violation in the Higgs sector, the resulting physical spectrum for the scalars is enlarged relative to the SM and includes light and heavy neutral CP-even Higgses (h^0 and H^0), charged Higgses ($H^\pm$), and a pseudoscalar A^0. In addition to the masses, two additional parameters are introduced in the theory: the ratio of the vevs of the two Higgs fields ($\tan\beta$), and the mixing of the two neutral CP-even Higgses ($\sin\alpha$).

There are many types of 2HDMs, each differing in the way the two Higgs doublets couple to the fermions (for a comprehensive review, see [6]). In this work, we will be concentrating on the Type II case, in which one Higgs doublet couples to the up-type quarks, while the other Higgs doublet couples to the down-type quarks and leptons. This model is of particular interest as it shares many of the features of the Higgs sector of the Minimal Supersymmetric Standard Model (MSSM). This enables us to translate existing LHC SUSY results to this case. Before proceeding, we point out that over the last few months, there have been various studies on the 2HDM based on the recent discovery [10–20]. While most studies concentrated on finding regions of parameter space that admit $\sigma\times$ Br values reported

by the LHC experiments in various channels, some also looked at correlations between the various decay channels. The authors of Ref. [10] and Ref. [11] did the initial study of looking at the $\tan\beta - \sin\alpha$ plane where the observed Higgs signal is feasible, interpreting the discovered scalar as either the light or the heavy CP-even Higgs boson. Ref. [12–16] fit the observed Higgs signals in various 2HDM scenarios, taken into account theoretical and experimental constraints. Ref. [17] also paid careful attention to various Higgs production modes. Ref. [18] focused on the CP-violating Type II 2HDM. Ref. [19] studied the case of nearly degenerate Higgs bosons. In addition, Ref. [20] investigated the possibility that the signal could correspond to the pseudoscalar A^0 - in this context, it is worth remarking that Ref. [21] considered the pseudoscalar interpretation of the observed 126 GeV resonance and found that while it is strongly disfavored, the possibility is not yet ruled out at the 5σ level.[1]

In the present paper, we extended the above analyses by combining all the known experimental constraints (the LEP, Tevatron and the LHC bounds) with the theoretical ones (perturbativity, unitarity, vacuum stability, and $\Delta\rho$), as well as flavor constraints. A unique aspect of the present work is that our analysis looks at combinations of all parameters of the theory to identify regions that survive all the theoretical and experimental constraints. We further focus on regions that could accommodate the observed Higgs signal as either the light or the heavy CP-even Higgs, and are thus interesting from a collider study perspective. This enables us to draw conclusions about correlations between different masses and mixing angles to help identify aspects of the model that warrant future study.

We start by briefly introducing the structure and parameters of the Type II 2HDM in Section II. In Sec. III, we discuss the theoretical constraints and experimental bounds, and outline our analysis methodology. In Sec. IV, we present our results for the light CP-even Higgs being the observed 126 GeV SM-like Higgs boson, looking at surviving regions in various combinations of free parameters. In Sec. V, we do the same for the heavy CP-even Higgs as the observed 126 GeV SM-like Higgs boson. In Sec. VI, we explore the implications for the Vector Boson Fusion (VBF) or VH associated production, and decays of Higgs into bb and $\tau\tau$ channels. We conclude in Section VII.

[1] The latest experimental results indicate that the pseudoscalar interpretation of the 126 GeV excess is disfavored [4, 5].

II. TYPE II 2HDM

In this section, we briefly describe the Type II 2HDM, focusing on the particle content, Higgs couplings, and model parameters. For more details about the model, see Ref. [6] for a recent review of the theory and phenomenology of 2HDM.

A. Potential, Masses and Mixing Angles

Labeling the two $\mathrm{SU}(2)_L$ doublet scalar fields Φ_1 and Φ_2, the most general potential in the Higgs sector can be written down in the following form:

$$\begin{aligned} V(\Phi_1,\Phi_2) = \quad & m_{11}^2\Phi_1^\dagger\Phi_1 + m_{22}^2\Phi_2^\dagger\Phi_2 - m_{12}^2(\Phi_1^\dagger\Phi_2 + \text{h.c.}) \\ & + \frac{1}{2}\lambda_1(\Phi_1^\dagger\Phi_1)^2 + \frac{1}{2}\lambda_2(\Phi_2^\dagger\Phi_2)^2 + \lambda_3(\Phi_1^\dagger\Phi_1)(\Phi_2^\dagger\Phi_2) + \lambda_4(\Phi_1^\dagger\Phi_2)(\Phi_2^\dagger\Phi_1) \\ & + \frac{1}{2}\Big\{\lambda_5(\Phi_1^\dagger\Phi_2)^2 + \text{h.c.}\Big\} + \Big\{\Big[\lambda_6(\Phi_1^\dagger\Phi_1) + \lambda_7(\Phi_2^\dagger\Phi_2)\Big](\Phi_1^\dagger\Phi_2) + \text{h.c.}\Big\}. \end{aligned} \quad (1)$$

We impose a discrete Z_2 symmetry on the Lagrangian, the effect of which is to render $m_{12}, \lambda_6, \lambda_7 = 0$[2]. After electroweak symmetry breaking (EWSB): $\langle\phi_1^0\rangle = v_1/\sqrt{2}$, $\langle\phi_2^0\rangle = v_2/\sqrt{2}$ with $\sqrt{v_1^2+v_2^2}$ =246 GeV, we are left with six free parameters, which can be chosen as the four Higgs masses (m_h, m_H, m_A, $m_{H^\pm}$), a mixing angle $\sin\alpha$ between the two CP-even Higgses, and the ratio of the two vacuum expectation values, $\tan\beta = v_2/v_1$.

Writing the two Higgs fields as:

$$\Phi_i = \begin{pmatrix} \phi_i^+ \\ (v_i + \phi_i^0 + iG_i)/\sqrt{2} \end{pmatrix} \quad (2)$$

the mass eigenstates of the physical scalars can be written as:

$$\begin{pmatrix} H^0 \\ h^0 \end{pmatrix} = \begin{pmatrix} \cos\alpha & \sin\alpha \\ -\sin\alpha & \cos\alpha \end{pmatrix} \begin{pmatrix} \phi_1^0 \\ \phi_2^0 \end{pmatrix}, \qquad \begin{aligned} A^0 &= -G_1\sin\beta + G_2\cos\beta \\ H^\pm &= -\phi_1^\pm\sin\beta + \phi_2^\pm\cos\beta \end{aligned}. \quad (3)$$

For our purposes, it is useful to express the quartic couplings $\lambda_{1\ldots5}$ in terms of the physical Higgs masses, $\tan\beta$ and the mixing angle α:

$$\lambda_1 = \frac{m_H^2\cos^2\alpha + m_h^2\sin^2\alpha}{v^2\cos^2\beta}, \qquad \lambda_2 = \frac{m_H^2\sin^2\alpha + m_h^2\cos^2\alpha}{v^2\cos^2\beta} \quad (4)$$

$$\lambda_3 = \frac{\sin 2\alpha(m_H^2 - m_h^2) + 2\,\sin 2\beta\, m_{H^\pm}^2}{v^2\,\sin 2\beta}, \qquad \lambda_4 = \frac{m_A^2 - 2m_{H^\pm}^2}{v^2}, \quad \lambda_5 = -\frac{m_A^2}{v^2}. \quad (5)$$

[2] Ref. [13], which also addresses similar issues as in this paper, allowed for a soft breaking of the Z_2 symmetry with $m_{12}^2 \neq 0$. In this paper, we don't consider such soft-breaking terms.

ξ_h^{VV}	$\sin(\beta-\alpha)$	ξ_H^{VV}	$\cos(\beta-\alpha)$	ξ_A^{VV}	0
ξ_h^{u}	$\cos\alpha/\sin\beta$	ξ_H^{u}	$\sin\alpha/\sin\beta$	ξ_A^{u}	$\cot\beta$
$\xi_h^{d,l}$	$-\sin\alpha/\cos\beta$	$\xi_H^{d,l}$	$\cos\alpha/\cos\beta$	$\xi_A^{d,l}$	$\tan\beta$

TABLE I: The multiplicative factor ξ by which the couplings of the CP-even Higgses and the CP-odd Higgs to the gauge bosons and fermions scale with respect to the SM value. The superscripts u, d, l and VV refer to the up-type quarks, down-type quarks, leptons, and WW/ZZ respectively.

The couplings of the CP-even Higgses and CP-odd Higgs to the SM gauge bosons and fermions are scaled by a factor ξ relative to the SM value – these are presented in Table I. In order to translate the ATLAS and CMS limits, we need to pay particular attention to the couplings of the light (heavy) CP-even Higgs to the SM gauge bosons (controlling the partial decay width of WW, ZZ as well as $\gamma\gamma$ channels) and to the top quark (controlling the gluon fusion production cross section), as well as to the bottom quark (controlling the bb partial decay width, which enters the total decay width as well). From Table I, we see that the relevant couplings are proportional to $\sin(\beta-\alpha)$ ($\cos(\beta-\alpha)$), $1/\sin\beta$ and $1/\cos\beta$. Thus, even though it is customary to look at the combination of parameters $(\sin\alpha, \tan\beta)$, we present our results in Sec. IV and V using $\sin(\beta-\alpha)$ and $\tan\beta$ as the independent parameters (in addition to the masses of the physical Higgses) to manifest the effects on the Higgs couplings to gauge bosons. Using $\sin(\beta-\alpha)$ instead of $\sin\alpha$ has the additional advantage of being basis-independent, as explained in Ref. [22].

III. CONSTRAINTS AND ANALYSES

A. Theoretical and Experimental Constraints

To implement the various experimental and theoretical constraints, we have employed two programs: the 2HDM Calculator (2HDMC) [23] to calculate the Higgs couplings, compute all the decay branching fractions of the Higgses, and implement all the theoretical constraints; and HiggsBounds 3.8 [24–26] to consistently put in all the experimental constraints on the model. Here, we briefly describe the list of theoretical and experimental bounds that are of interest.

Theoretical Constraints:

- Vaccuum Stability: This implies that the potential should be bounded from below, which is translated to various conditions for the quartic couplings in the Higgs potential [27]: $\lambda_1 > 0$, $\lambda_2 > 0$, $\lambda_3 > -\sqrt{\lambda_1 \lambda_2}$, and $\lambda_3 + \lambda_4 - |\lambda_5| > -\sqrt{\lambda_1 \lambda_2}$. With Eqs. (4) and (5), the above requirements serve to constrain the Higgs masses and angles.

- Perturbativity: 2HDMC imposes constraints on the physical Higgs quartic couplings, specifically demanding that $\lambda_{h_i h_j h_k h_l} < 4\pi$ to stay inside the perturbative regime. Note that even though these are different from the λs in the Higgs potential in Eq. (1), we can still use Eqs. (4) and (5) as rough guides to understand the perturbative bounds, as we will do in later sections to explain the features of our results.

- Unitarity: It is well known that in the SM, the scattering cross section for the longitudinal W modes is unitary only if the Higgs exchange diagrams are included. Since the couplings of the Higgs are modified in the 2HDM, we need to ensure unitarity by demanding that the S matrix of *all* scattering cross sections of Higgs$-$Higgs and Higgs$-V_L$ (where V_L is either W_L or Z_L) have eigenvalues bounded by 16π [28].

- $\Delta\rho$: The ρ parameter is defined as $\rho \equiv \frac{m_W^2}{m_Z^2 \cos^2\theta_W}$, where θ_W is the Weinberg angle. The tree level value for ρ is one in the SM, while it receives radiative correction from both the SM sector and new physics. ρ has been measured very precisely via Z-pole precision observables to be very close to one [29], which imposes a strong constraint on the amount of custodial symmetry breaking in the new physics sector. In the case of 2HDM, the mass difference between the various Higgses are therefore highly constrained [30], which leads to interesting correlations between some of the masses, as will be demonstrated in Sec. IV and Sec. V.

Experimental Constraints: The LHC experiments have searched for the SM Higgs in $\gamma\gamma$, ZZ, WW, $\tau\tau$ and bb channels. Both the ATLAS and CMS collaboration have reported the observation of a new resonance at a mass of around 126 GeV with more than 5σ significance [1–4, 31, 32]. The production cross sections and partial decay widths of the 2HDM Higgses to the various SM final states differ from that of the SM Higgs, which can be obtained using the coupling scaling factors ξ from Table I. Thus, we can identify the regions in parameter space where the signal cross sections are compatible with the Higgs

signal observed at the ATLAS and CMS collaborations. We can also translate the exclusion bounds on the Higgs search to the ones in the 2HDM. We used HiggsBounds 3.8 to impose the exclusion limits from Higgs searches at the LEP and the Tevatron [33–37]. We also incorporated the latest Higgs search results at the LHC [2, 4, 31, 32, 38, 39].

We also considered flavor constraints to show the effects on the available parameter spaces once bounds from flavor sector are imposed in addition to the ones described. To do this, we employed the program SuperIso 3.3 [40], which incorporates, among other things, bounds from $B \to X_s\gamma$, ΔM_{B_d}, $D_s \to \tau\nu_\tau$ and $B \to \mu^+\mu^-$ [41–43]. A summary of flavor bounds can be found in Ref. [44]. Flavor constraints on the Higgs sector are, however, typically more model-dependent. Therefore, our focus in this work is mainly on the implication of the Higgs search results on the Type II 2HDM, and we only impose the flavor bounds at the last step to indicate how the surviving regions further shrink.

B. Analysis Method

In our analyses, we considered two scenarios:

- h^0-126 case with $m_h = 126$ GeV,
- H^0-126 case with $m_H = 126$ GeV.

and scanned over the entire remaining parameter space varying m_H (or m_h), m_A, m_{H^+}, $\tan\beta$ and $\sin(\beta-\alpha)$:

$$
\begin{aligned}
20\text{ GeV} \le\ & m_A, m_{H^\pm} && \le 900\text{ GeV} && \text{in steps of 20 GeV}, && (6)\\
-1 \le\ & \sin(\beta-\alpha) && \le 1 && \text{in steps of 0.05}, && (7)\\
\mathbf{h^0-126\ case}:\ 0.25 \le\ & \tan\beta && \le 5 && \text{in steps of 0.25}, && (8)\\
126\text{ GeV} \le\ & m_H && \le 900\text{ GeV} && \text{in steps of 20 GeV}, && (9)\\
\mathbf{H^0-126\ case}:\ 1 \le\ & \tan\beta && \le 30 && \text{in steps of 1}, && (10)\\
6\text{ GeV} \le\ & m_h && < 126\text{ GeV} && \text{in steps of 5 GeV}. && (11)
\end{aligned}
$$

We used the 2HDMC 1.2beta [23] which tested if each parameter point fulfills the theoretical and experimental constraints implemented in HiggsBounds 3.8. New LHC results that are not included in HiggsBounds 3.8 were implemented in addition. We further required either h^0

or H^0 to satisfy the cross section requirement for $\gamma\gamma$, WW and ZZ channels to accommodate the observed Higgs signal:

$$0.9 < \frac{\sigma(gg \to h^0/H^0 \to \gamma\gamma)}{\sigma_{\rm SM}} < 2.2, \quad 0.2 < \frac{\sigma(gg \to h^0/H^0 \to WW/ZZ)}{\sigma_{\rm SM}} < 1.4. \qquad (12)$$

The lower end of the ranges come from the lower limits of 95% C.L. range for the observed Higgs signal strength [2, 4], while the upper end of the ranges come from the 95% C.L. exclusion bounds from Higgs searches [31, 32], which are stronger than the 95% C.L. signal range. In the last step we imposed the flavor bounds on all points that satisfy Eq. (12) using the SuperIso 3.3 program to study the consequence of the flavor constraints.

IV. LIGHT HIGGS AT 126 GEV

A. Cross sections and Correlations

Before presenting the results of the numerical scanning of parameter regions with all the theoretical and experimental constraints imposed, let us first study the $\tan\beta$ and $\sin(\beta-\alpha)$ dependence of the cross sections for the major search channels at the LHC: $gg \to h^0 \to \gamma\gamma, WW/ZZ$. Both production cross sections and decay branching fractions are modified relative to the SM values:

$$\frac{\sigma \times {\rm Br}(gg \to h^0 \to XX)}{\rm SM} = \frac{\sigma(gg \to h^0)}{\sigma_{\rm SM}} \times \frac{{\rm Br}(h^0 \to XX)}{{\rm Br}(h_{\rm SM} \to XX)}, \qquad (13)$$

for $XX = \gamma\gamma, VV$. Note that since the WW and ZZ couplings are modified the same way in the Type II 2HDM, we use VV to denote both WW and ZZ channels.

The ratio of the gluon fusion cross section normalized to the SM value can be written as:

$$\frac{\sigma(gg \to h^0)}{\sigma_{\rm SM}} = \frac{\cos^2\alpha}{\sin^2\beta} + \frac{\sin^2\alpha}{\cos^2\beta}\frac{|A_{1/2}(\tau_b)|^2}{|A_{1/2}(\tau_t)|^2} \qquad (14)$$

$$= \left[\frac{\cos(\beta-\alpha)}{\tan\beta} + \sin(\beta-\alpha)\right]^2 + \left[\cos(\beta-\alpha)\tan\beta - \sin(\beta-\alpha)\right]^2 \frac{|A_{1/2}(\tau_b)|^2}{|A_{1/2}(\tau_t)|^2} \qquad (15)$$

The expression for the fermion loop functions $A_{1/2}(\tau_{t,b})$ can be found in Ref. [30]. The first term in Eq. (14) is the top-loop contribution, and the second term is the bottom-loop contribution. In the SM, the top-loop contributes dominantly to the gluon fusion diagram, while the bottom-loop contribution is negligibly small. The situation alters in type II 2HDM for large $\tan\beta$, when the bottom-loop contribution can be substantial due to the enhanced

bottom Yukawa [10]. We also rewrite it in $\sin(\beta-\alpha)$, $\cos(\beta-\alpha)$ and $\tan\beta$ in Eq. (15) to make their dependence explicit.

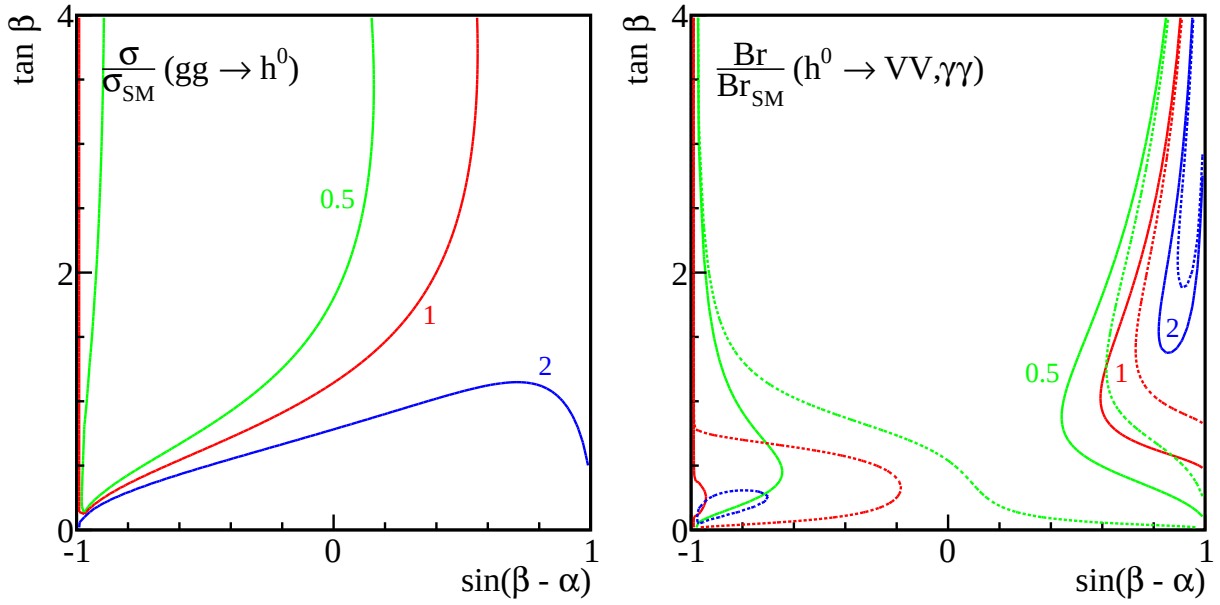

FIG. 1: The normalized $gg \to h^0$ production cross section contours (left panel) and $h^0 \to VV$ (solid lines of the right panel) and $h^0 \to \gamma\gamma$ (dashed lines of the right panel) branching fractions in the h^0-126 case. The contour lines are $\sigma/\sigma_{\rm SM}$, $\mathrm{Br}/\mathrm{Br}_{\rm SM} = 0.5$ (green), 1 (red), and 2 (blue).

In the left panel of Fig. 1, we show contours of $\sigma/\sigma_{\rm SM}$ for the gluon fusion: $\sigma/\sigma_{\rm SM} = 0.5$ (green), 1 (red), and 2 (blue). While contours of $\sigma/\sigma_{\rm SM} \geq 1$ accumulate in $\sin(\beta-\alpha) \sim -1$ region, there is a wide spread of the contours for $\sin(\beta-\alpha) > 0$. For most regions of $\sin(\beta-\alpha) < 0$, $gg \to h^0$ is suppressed compared to the SM value due to cancellations between the $\cos(\beta-\alpha)$ and $\sin(\beta-\alpha)$ terms in the top Yukawa coupling, as shown in Eq. (15). Note that we have shown the plots only for $\tan\beta \leq 4$ since the model is perturbatively valid only for $\tan\beta \lesssim 4$, as will be demonstrated below in the results of the full analysis.

The h^0 decay branching fractions $h^0 \to VV, \gamma\gamma$ can be written approximately as

$$\frac{\mathrm{Br}(h^0 \to XX)}{\mathrm{Br}(h_{\rm SM} \to XX)} = \frac{\Gamma_{XX}}{\Gamma_{total}} \times \frac{\Gamma^{\rm SM}_{total}}{\Gamma^{\rm SM}_{XX}} \approx \begin{cases} \dfrac{\sin^2(\beta-\alpha)}{\sin^2(\beta-\alpha)\mathrm{Br}(h_{\rm SM}\to VV)+\frac{\sin^2\alpha}{\cos^2\beta}\mathrm{Br}(h_{\rm SM}\to bb)+\ldots} \\ \dfrac{\Gamma(h^0\to\gamma\gamma)/\Gamma(h_{\rm SM}\to\gamma\gamma)}{\sin^2(\beta-\alpha)\mathrm{Br}(h_{\rm SM}\to VV)+\frac{\sin^2\alpha}{\cos^2\beta}\mathrm{Br}(h_{\rm SM}\to bb)+\ldots} \end{cases}, \qquad (16)$$

where we have explicitly listed the dominant bb and WW/ZZ channels and used "$+\ldots$" to indicate other sub-dominant SM Higgs decay channels.

In the right panel of Fig. 1, we show contours of $\mathrm{Br}/\mathrm{Br}_{\rm SM}$ for VV (solid lines) and $\gamma\gamma$

(dashed lines) channels. Both VV and loop induced (dominantly W-loop) $\gamma\gamma$ channels exhibit similar parameter dependence on $\tan\beta$ and $\sin(\beta-\alpha)$ since both channels are dominantly controlled by the same h^0VV coupling. While contours of $\mathrm{Br}/\mathrm{Br}_{\mathrm{SM}} \gtrsim 1$ appear near $\sin(\beta-\alpha) \sim \pm 1$ for unsuppressed h^0VV couplings, $h^0 \to \gamma\gamma$ shows some spread for negative $\sin(\beta-\alpha)$ and small $\tan\beta$ due to the correction to top Yukawa in the loop-indued $h^0\gamma\gamma$ coupling.

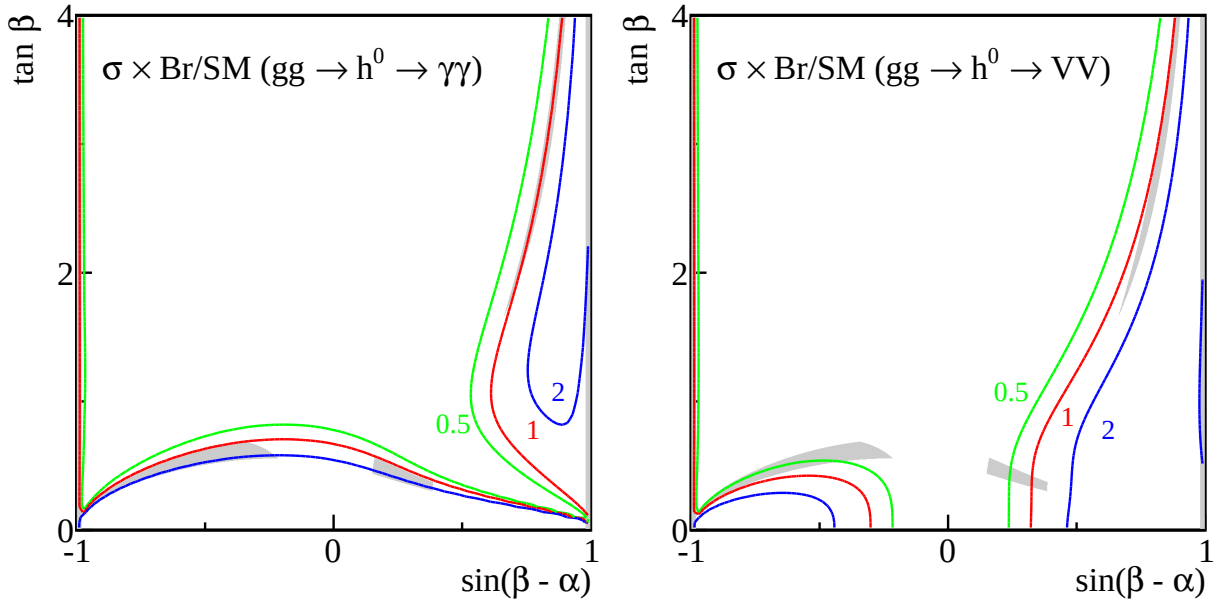

FIG. 2: $\sigma \times \mathrm{Br}/\mathrm{SM}$ for the processes $gg \to h^0 \to \gamma\gamma$ (left), and $gg \to h^0 \to WW/ZZ$ (right) in the h^0-126 case. The contour lines are $\sigma \times \mathrm{Br}/\mathrm{SM} = 0.5$ (green), 1 (red), and 2 (blue). The shaded gray are regions where cross sections of $\gamma\gamma$ and WW/ZZ channels satisfy Eq. (12).

Combining both the production and the decay branching fractions, we present the contours of $\sigma \times \mathrm{Br}/\mathrm{SM}$ in Fig. 2 for $\gamma\gamma$ (left panel) and VV (right panel) for $\sigma \times \mathrm{Br}/\mathrm{SM} = 0.5$ (green), 1 (red), and 2 (blue). Once we demand that the cross sections for these processes be consistent with the experimental observation of a 126 GeV Higgs, as given in Eq. (12), the allowed regions of parameter space split into five distinct regions, as indicated by the shaded gray areas. There are two narrow regions one each at $\sin(\beta-\alpha) = \pm 1$ (the gray regions overlap with the picture frame boundary therefore hard to see), one region near $\sin(\beta-\alpha) = +1$, and two extended regions spanning the entire range of $\sin(\beta-\alpha)$ for $\tan\beta < 1$. In what follows, we will display separate plots for positive and negative $\sin(\beta-\alpha)$ to show the different features that appear in these two cases.

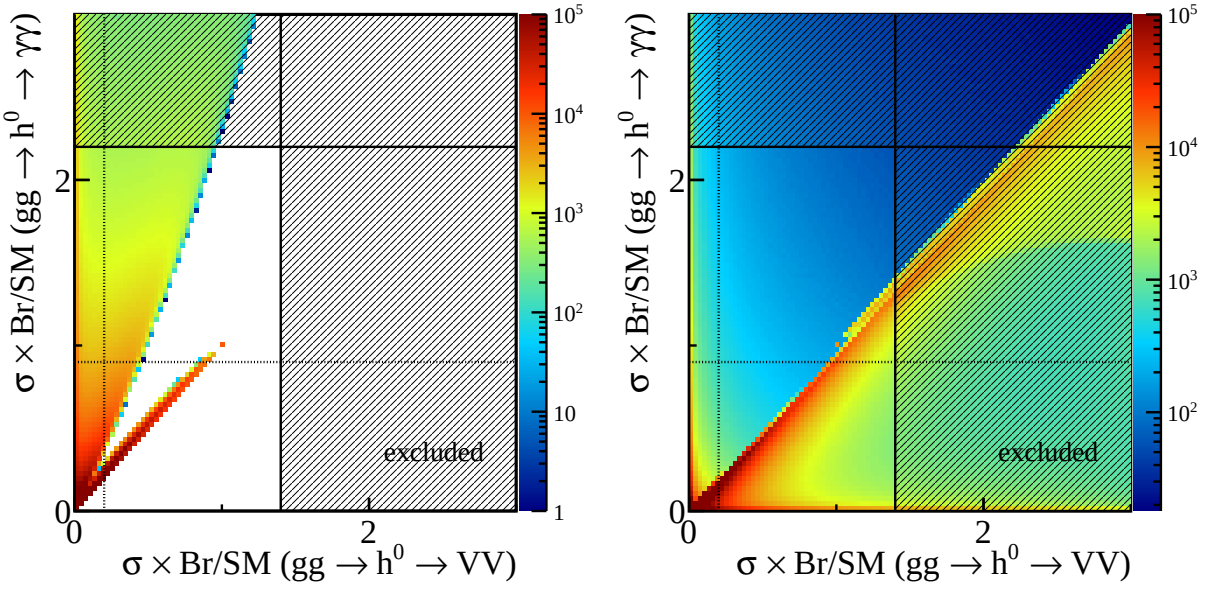

FIG. 3: $\sigma \times$ Br/SM for $gg \to h^0 \to \gamma\gamma$ versus $gg \to h^0 \to VV$ for negative $\sin(\beta - \alpha)$ (left panel), and positive $\sin(\beta - \alpha)$ (right panel) in the h^0-126 case. Color map indicates the density of points with red being the most dense region and blue being the least dense region. The hatched region is excluded by the current Higgs searches in the $\gamma\gamma$, WW and ZZ channel at 95% C.L. [31, 32]. The horizontal and vertical dashed lines indicate the lower end of the normalized signal cross section ranges of $\gamma\gamma$ and VV channels being 0.9 and 0.2, respectively [2, 4].

In Fig. 3, we show the correlations for $\sigma \times$ Br/SM for the $\gamma\gamma$ channel against VV, for negative (positive) values of $\sin(\beta - \alpha)$ in the left (right) panel as a density plot. Color coding is such that the points in red are the most dense (i.e., most likely) and points in blue are the least dense (i.e., less likely). For negative $\sin(\beta - \alpha)$, there are two branches: one region (more likely) along the diagonal line with $\gamma\gamma : VV \sim 1$ and $\sigma_{\gamma\gamma} \lesssim 1$; another region (less likely) in the upper-half plane where $\gamma\gamma : VV \gtrsim 2$ and $\sigma_{\gamma\gamma}$ extends to 2 or larger. These can be mapped on to specfic regions in Fig. 2 – while the diagonal region corresponds to the $\sin(\beta - \alpha) = -1$ branch, the other branch in which the VV is suppressed relative to $\gamma\gamma$ corresponds to the extended $\sin(\beta - \alpha)$ region with small $\tan\beta$.

For positive values of $\sin(\beta - \alpha)$, the diagonal region is most probable, with $\gamma\gamma : VV \sim 1$ and $\sigma_{\gamma\gamma}$ possibly extending over a large range. Branches with $\sigma_{\gamma\gamma}$ or $\sigma_{VV} \sim 0$ are strongly disfavored given the current observation of the Higgs signal.

Superimposed on both figures are the latest ATLAS and CMS results on the windows of

cross sections for $\gamma\gamma$, WW and ZZ as given in Eq. (12). Note that these signal windows are also sketched in Fig. 2 as the shaded gray regions. Concentrating on the regions favored by experiments (bounded by the horizontal and vertical lines in Fig. 3), we see that in the $\sin(\beta-\alpha) < 0$ case, the most likely regions are the ones with $\gamma\gamma : VV \sim 1$ and $\sigma_{\gamma\gamma} \sim 1$. About an order of magnitude less likely is the region with $\gamma\gamma : VV \gtrsim 2$ and $\sigma_{\gamma\gamma} \gtrsim 0.9$ and $\sigma_{VV} \gtrsim 0.4$. For positive values of $\sin(\beta-\alpha)$, the most likely region is the one where $\gamma\gamma : VV \sim 1$ with $\sigma_{\gamma\gamma,VV}$ between 0.9 to 1.4.

Thus we see that for all values of $\sin(\beta-\alpha)$, the VV and $\gamma\gamma$ channels are highly positively correlated[3] and this fact serves as an important piece of discrimination for this model as more data is accumulated. Most of the points falls into $\gamma\gamma : VV \sim 1$ with the cross section of both around the SM strength. It is possible, though very unlikely, that there are regions in negative $\sin(\beta-\alpha)$ and small $\tan\beta < 1$ with $\gamma\gamma : VV \gtrsim 2$ and possible significant enhancement of the $\gamma\gamma$ rate over the SM value.

The above analyses illustrate the cross section and decay branching fraction behavior of the light CP-even Higgs when it is interpreted as the observed 126 GeV SM-like Higgs, using the approximate formulae in Eqs. (14) - (16). Note that we have only included the usual SM Higgs decay channels in Γ_{tot} in Eq. (16). While it is a valid approximation in most regions of the parameter space, it might break down when light states in the spectrum open up new decay modes or introduce large loop contributions to either $gg \to h^0$ or $h^0 \to \gamma\gamma$. In our full analysis presented below with scanning over the parameter spaces, we used the program 2HDMC, which takes into account all the decay channels of the Higgs, as well as other loop corrections to the gluon fusion production or Higgs decays to $\gamma\gamma$.

B. Parameter spaces

Fixing $m_h = 126$ GeV still leaves us with five parameters: three masses, $m_H, m_A, m_{H^\pm}$, and two angles $\tan\beta$ and $\sin(\beta-\alpha)$. Varying those parameters in the ranges given in Eqs. (6)-(9), we study the remaining parameter regions satisfying all the theoretical and experimental constraints as well as regions that are consistent with the observed Higgs signal.

The left panel of Fig. 4 shows the viable regions in $\tan\beta$ versus $\sin(\beta-\alpha)$ plane when

[3] This agrees with the results of [13].

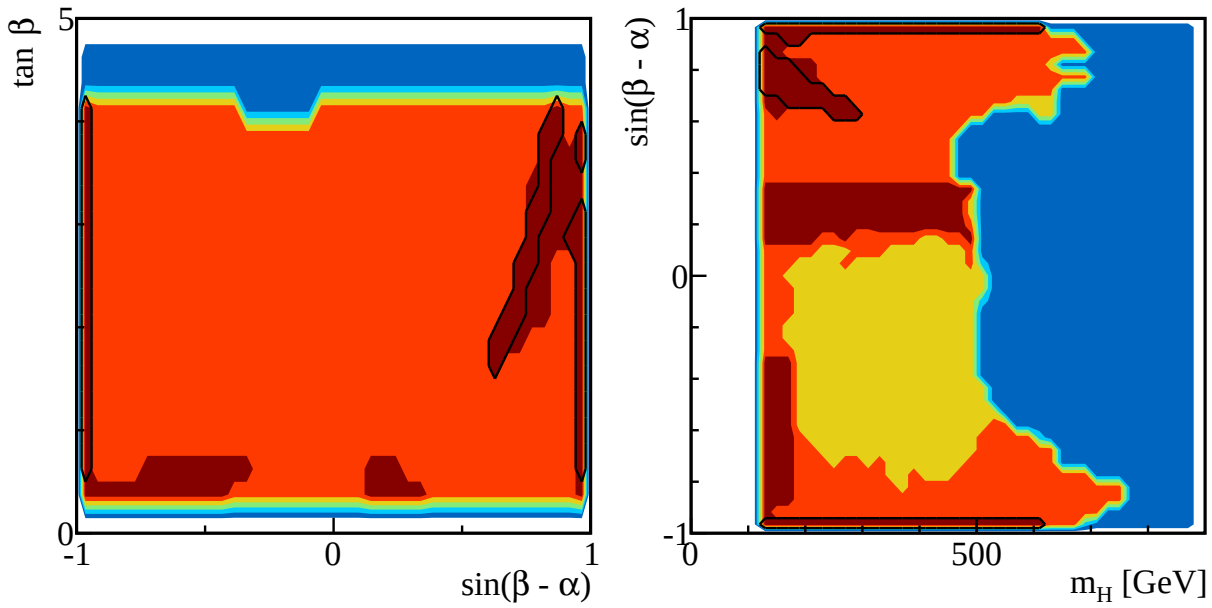

FIG. 4: Parameter regions in the h^0-126 case for $\tan\beta$ versus $\sin(\beta-\alpha)$ (left panel) and $\sin(\beta-\alpha)$ versus m_H (right panel). We show regions excluded by stability, unitarity and perturbativity (dark blue), $\Delta\rho$ (light blue), LEP results (green), Tevatron and LHC results (yellow). Regions that survive all the theoretical and experimental constraints are shown in red. Also shown in dark red are regions consistent with the light CP-even Higgs interpreted as the observed 126 GeV scalar resonance, satisfying the cross section requirement of Eq. (12) for $gg \to h^0 \to \gamma\gamma, WW/ZZ$. Regions enclosed by the black curves are the ones that survive the flavor constraints.

various theoretical constraints and experimental exclusions are imposed sequentially. The red regions are those that satisfy all the constraints. Also shown in dark red are regions consistent with the light CP-even Higgs interpreted as the observed 126 GeV scalar particle, satisfying the cross section requirement of Eq. (12) for $gg \to h^0 \to \gamma\gamma, WW/ZZ$. The signal regions (two narrow regions at $\sin(\beta-\alpha) = \pm 1$, one region near $\sin(\beta-\alpha) = 1$ and two extended regions for $\tan\beta < 1$) agree well with the shaded region in Fig. 2. Regions with $\tan\beta \gtrsim 4$ are excluded by perturbative bounds since one of $\lambda_{1,2}$ becomes non-perturbative for larger value of $\tan\beta$ ($\cos\beta \to 0$), as shown in Eq. (4). Consequently, the bottom loop contribution to the gluon fusion production cross section [6] is not a major factor for the h^0-126 case.

To further explore the flavor constraints, we show in Fig. 4 the regions enclosed by the black curves being those that survive the flavor bounds. We see that the flavor constraints

reduce the five signal regions down to three. The extended regions around $\tan\beta < 1$ are disfavored by flavor consideration, which agree with previous works [15, 44]. Regions near $\sin(\beta-\alpha) \sim \pm 1$ still remain viable after all the considerations.

The right panel of Fig. 4 shows the allowed region in the $\sin(\beta-\alpha)-m_H$ plane. Imposing all the theoretical constraints, in particular, the perturbativity requirement, translates into an upper bound on m_H of around 750 GeV. Higgs search bounds from the LHC removes a large region in negative $\sin(\beta-\alpha)$, mostly from the stringent bounds from WW and ZZ channels for the heavy Higgs. The positive $\sin(\beta-\alpha)$ region is less constrained since $gg \to H^0 \to WW/ZZ$ are much more suppressed. Requiring h^0 to fit the observed Higgs signal further narrows down the favored region, as shown in dark red. For $\sin(\beta-\alpha) = \pm 1$, m_H could be as large as 600 GeV. For $0.6 \lesssim \sin(\beta-\alpha) \lesssim 1$, m_H is constrained to be less than 300 GeV. For the extended region of $0.1 \lesssim \sin(\beta-\alpha) \lesssim 0.4$, m_H extends to around 500 GeV, while for $-1 \lesssim \sin(\beta-\alpha) \lesssim -0.3$, m_H is restricted to be less than 180 GeV. Imposing the flavor constraints further narrows down the regions to strips at $\sin(\beta-\alpha) = \pm 1$ and a region at $0.6 \lesssim \sin(\beta-\alpha) \lesssim 1$. The correlation between m_H and $\sin(\beta-\alpha)$ indicates that if a heavy CP-even Higgs is found to be between 500 and 600 GeV, $\sin(\beta-\alpha)$ is constrained to be very close to ± 1, indicating the light Higgs having SM-like couplings to the gauge sector.

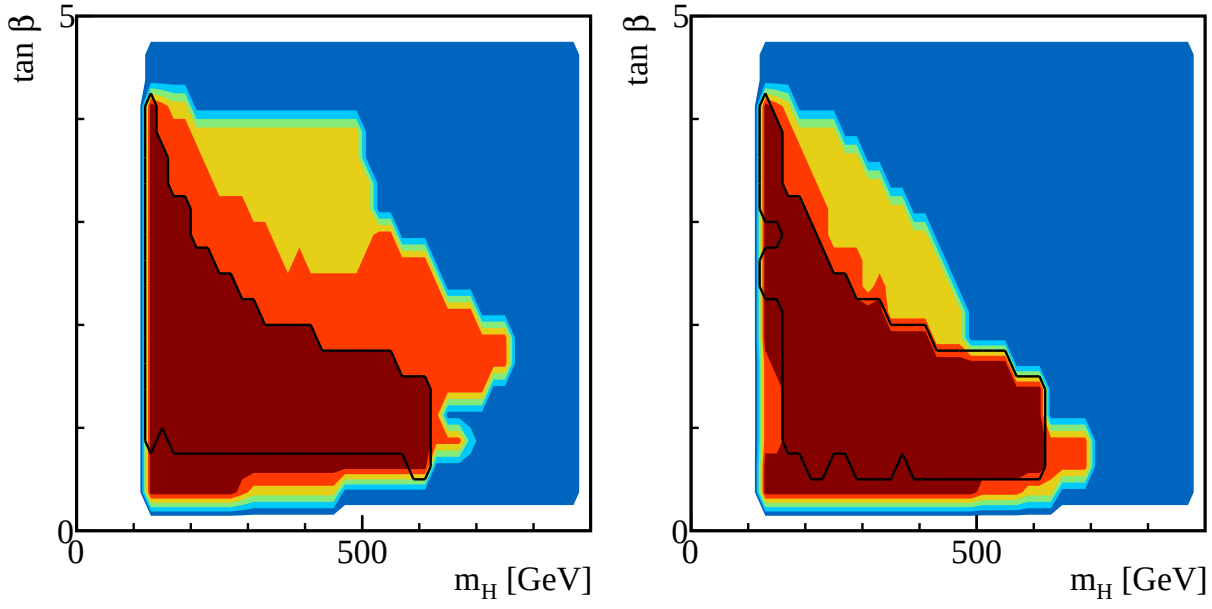

FIG. 5: Parameter regions in the h^0-126 case for $\tan\beta$ versus m_H with $\sin(\beta-\alpha) < 0$ (left panel) and $\sin(\beta-\alpha) > 0$ (right panel). Color coding is the same as Fig. 4.

In Fig. 5, we present the parameter regions for $\tan\beta$ versus m_H with $\sin(\beta-\alpha) < 0$ (left panel) and $\sin(\beta-\alpha) > 0$ (right panel). Regions with large m_H are typically realized for small $\tan\beta$ roughly between 1 and 2. There are also noticeable difference for positive or negative $\sin(\beta-\alpha)$ for regions that survive all the experimental constraints (red regions). Negative $\sin(\beta-\alpha)$ allows larger values of $\tan\beta$ for a given mass of m_H. Small values of $\tan\beta$ is disfavored by the flavor constraints, in particular, Δm_{B_d}, as pointed out in Ref. [44].

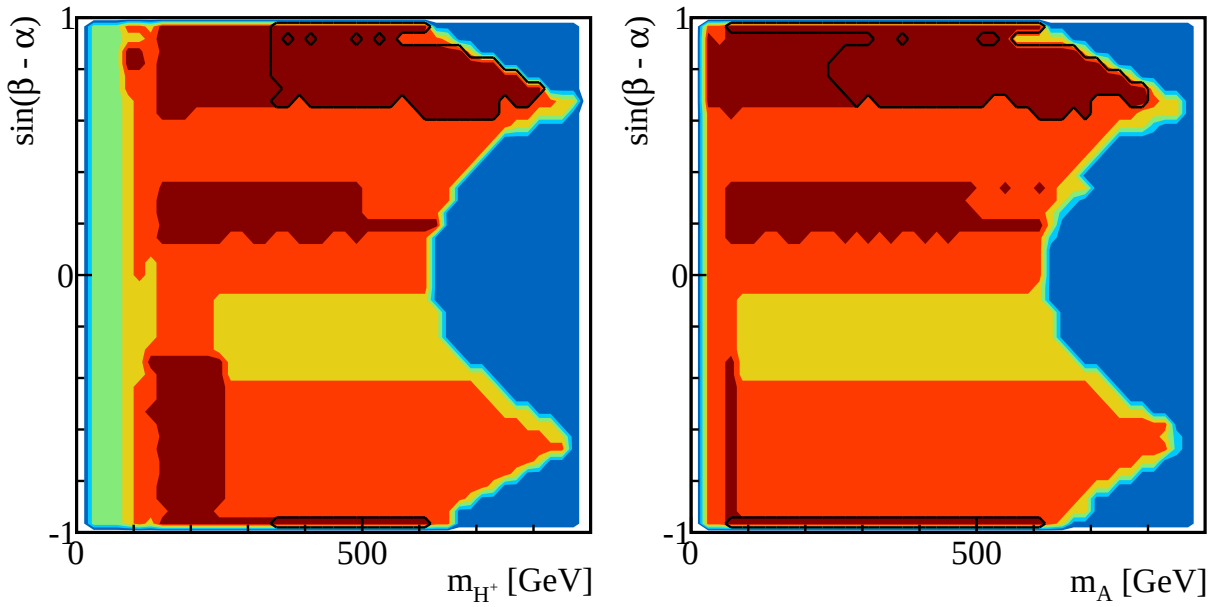

FIG. 6: Parameter regions in the h^0-126 case for $\sin(\beta-\alpha)$ versus $m_{H^\pm}$ (left panel) and m_A (right panel). Color coding is the same as Fig. 4.

Fig. 6 shows the parameter regions in $\sin(\beta-\alpha)$ versus $m_{H^\pm}$ (left panel) and m_A (right panel). The signal regions exhibit similar features as the $\sin(\beta-\alpha)$ versus m_H plot in the right panel of Fig. 4. Note that for negative $\sin(\beta-\alpha)$ between -0.4 to -0.1, only regions with $m_A < 60$ GeV survive the LHC Higgs search bounds. This is because $H^0 \to A^0A^0$ open up in this region, which leads to the suppression of $H^0 \to WW/ZZ$ to escape the experimental constraints. The corresponding surviving region in 120 GeV $< m_{H^\pm} <$ 250 GeV is introduced by the correlation between m_A and $m_{H^\pm}$ due to $\Delta\rho$ constraints. Imposing the cross section requirement for h^0 to satisfy the Higgs signal region results in four bands in both m_A and $m_{H^\pm}$. Only small $m_A \sim 60$ GeV, and $m_{H^\pm}$ between 120 and 250 GeV are allowed in the extended region in negative $\sin(\beta-\alpha)$, while larger values for m_A and $m_{H^\pm}$ can appear in the other regions. Imposing the flavor constraints leaves $m_{H^\pm} \gtrsim 300$ GeV

open with $\sin(\beta-\alpha)=\pm1$ or $\sin(\beta-\alpha)$ between 0.6 and 1, while smaller values for m_A remain viable at $\sin(\beta-\alpha)=\pm1$.

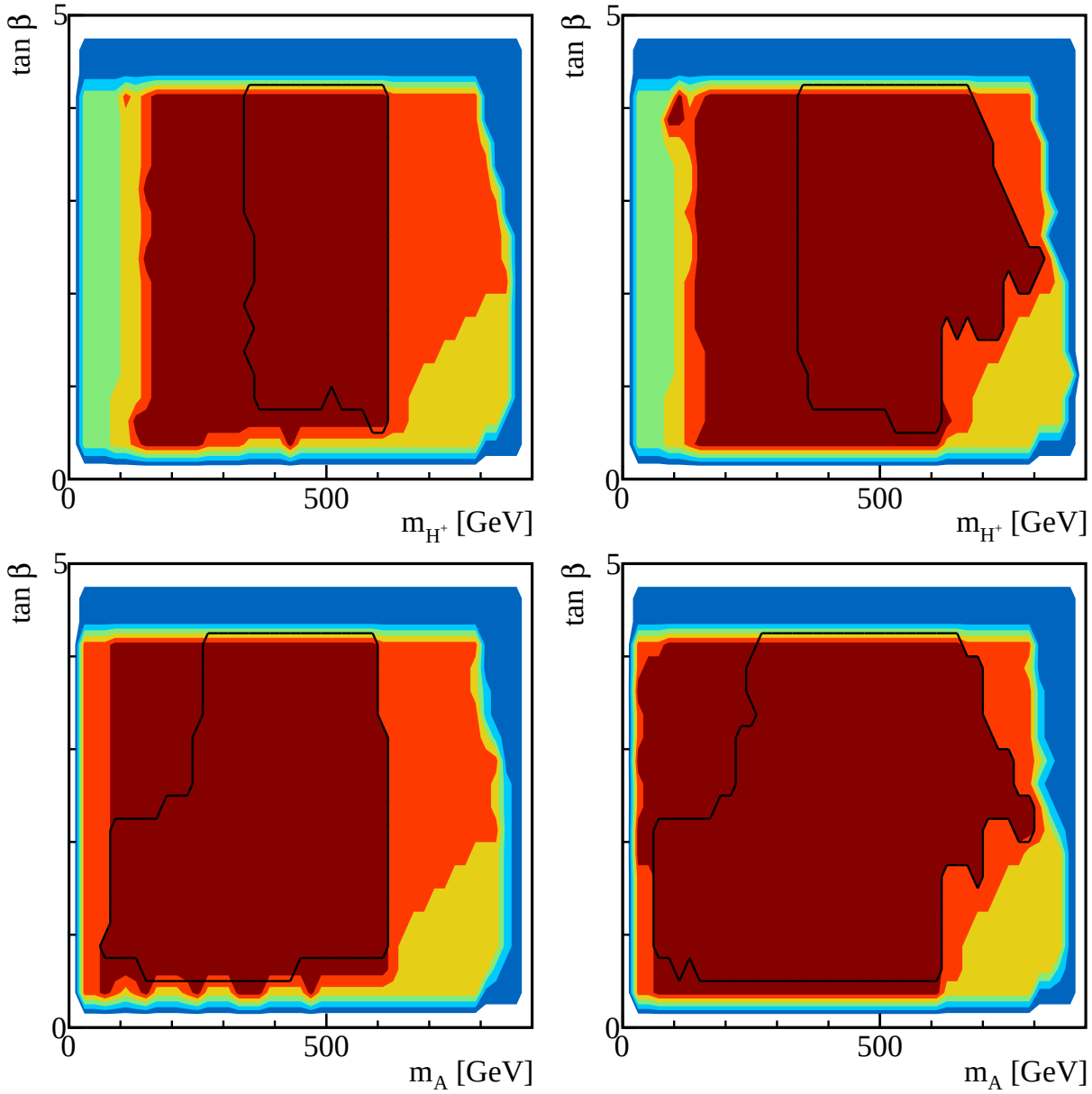

FIG. 7: Parameter regions in the h^0-126 case for $\tan\beta$ versus $m_{H^\pm}$ (top panels) and m_A (lower panels) with $\sin(\beta-\alpha)<0$ (left panels) and $\sin(\beta-\alpha)>0$ (right panels). Color coding is the same as Fig. 4.

The allowed regions in the $\tan\beta - m_{H^\pm}$ and $\tan\beta - m_A$ planes share similar features before flavor constraints are taken into account, which are shown in Fig. 7. The top two panels show the allowed regions in the $\tan\beta - m_{H^\pm}$ plane for negative and positive $\sin(\beta-\alpha)$,

while the lower two panels are for $\tan\beta - m_A$. LEP places a lower bound on the charged Higgs mass around 80 GeV [35, 36]. In the signal region for $\sin(\beta-\alpha) < 0$, both $m_{H^\pm}$ and m_A are less than about 600 GeV, while their masses could be extended to 800 GeV for $\sin(\beta-\alpha) > 0$ and $\tan\beta > 1.5$. The difference between the m_A range for different signs of $\sin(\beta-\alpha)$ can be explained as follows: regions with $m_A > 600$ GeV can only occur for $|\sin(\beta-\alpha)|$ between 0.4 and 0.8, as shown in the right panel of Fig. 6. The Higgs signal region of $\tan\beta$ versus $\sin(\beta-\alpha)$ (left panel of Fig. 4) shows that to simultaneously satisfy both the $\tan\beta$ range and $\sin(\beta-\alpha)$ range, only positive $\sin(\beta-\alpha)$ case survives.

Flavor bounds, as expected, have a marked effect here ruling out any value of $m_{H^\pm} < 300$ GeV for all values of $\tan\beta$, mainly due to the $b \to s\gamma$ constraint. For the CP-odd Higgs, only a corner of $\tan\beta > 2$ and $m_A < 300$ GeV is excluded, due to the combination of flavor and $\Delta\rho$ constraints. As shown in Fig. 5, only relatively light $m_H \lesssim 300$ GeV is allowed for $\tan\beta > 2$. The flavor constraints of $m_{H^\pm} \gtrsim 300$ GeV is then translated to $m_A \gtrsim 300$ GeV since the difference between m_A and $m_{H^\pm}$ is constrained by $\Delta\rho$ considerations when both m_h and m_H are relatively small. For $\tan\beta < 2$, m_H could be relatively high, which cancels the large contribution to $\Delta\rho$ from large $m_{H^\pm}$ while allowing m_A to be light.

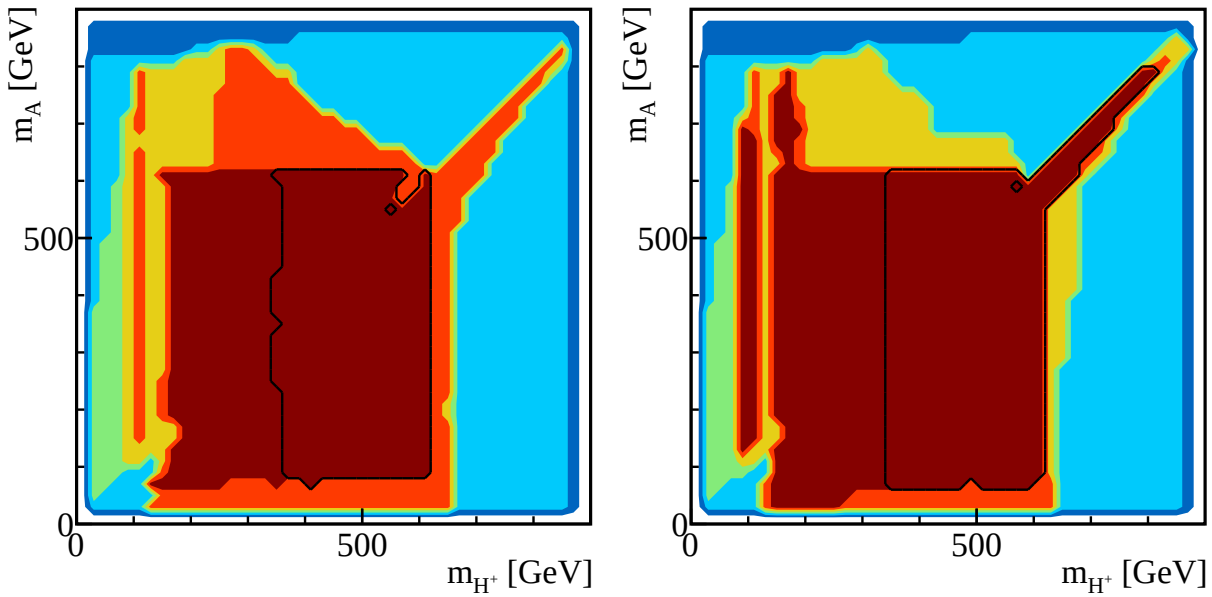

FIG. 8: Parameter regions in the h^0-126 case for m_A versus $m_{H^\pm}$ with $\sin(\beta-\alpha) < 0$ (left panel) and $\sin(\beta-\alpha) > 0$ (right panel). Color coding is the same as Fig. 4.

In Fig. 8, we present the parameter regions in the $m_A - m_{H^\pm}$ plane for negative and

positive values of $\sin(\beta-\alpha)$. m_A and $m_{H^\pm}$ are uncorrelated for most parts of the parameter space. For $\sin(\beta-\alpha)>0$ when $m_{A,H^\pm}$ could reach values larger than 600 GeV, $\tan\beta$ is at least 1.5 or larger (see Fig. 7). m_H is restricted to less than 300 GeV in this region, which results in a strong correlation between m_A and $m_{H^\pm}$ due to the $\Delta\rho$ constraints.

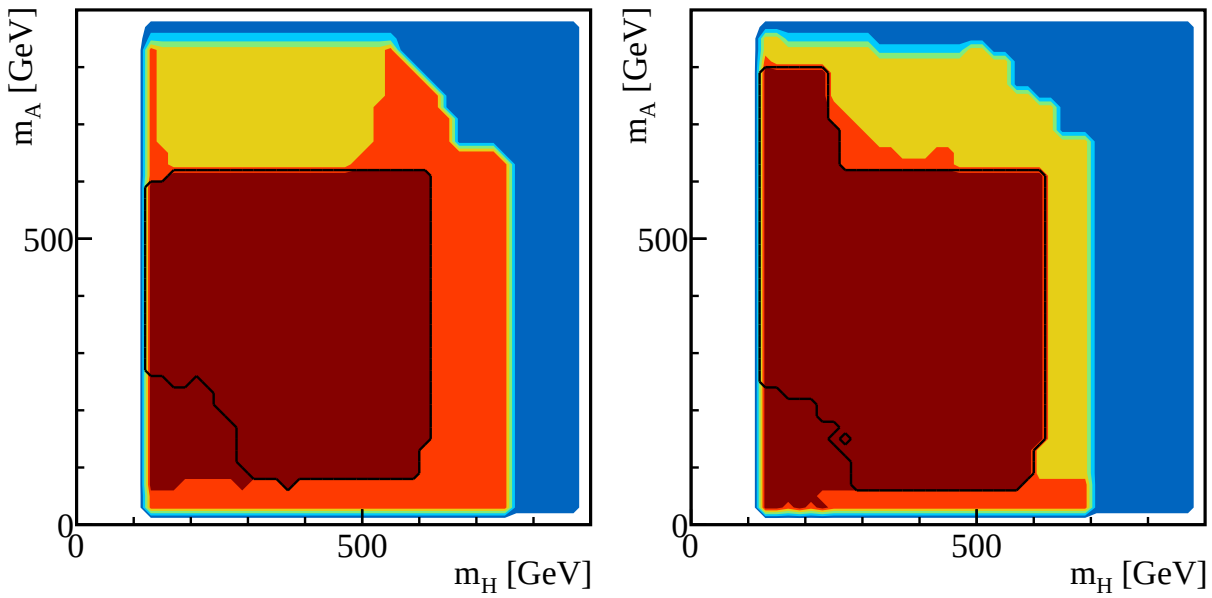

FIG. 9: Parameter regions in the h^0-126 case for m_A versus m_H with $\sin(\beta-\alpha)<0$ (left panel) and $\sin(\beta-\alpha)>0$ (right panel). Color coding is the same as Fig. 4.

Fig. 9 shows the parameter space in the $m_A - m_H$ plane for negative (left panel) and positive (right panel) $\sin(\beta-\alpha)$. These two masses are largely uncorrelated for either sign of $\sin(\beta-\alpha)$. Note that for $\sin(\beta-\alpha)>0$, large m_A between $600-800$ GeV is only possible for small values of $m_H \lesssim 300$ GeV. This is because the corresponding $\tan\beta$ is larger than 1.5, which bounds m_H from above. The lower-left corners excluded by flavor constraints correspond to the upper-left corners in $m_A - \tan\beta$ plots in Fig. 7, since at least one of m_A or m_H would need to be relatively heavy to cancel the contribution to $\Delta\rho$ from $m_{H^\pm} > 300$ GeV.

We conclude this section with the following comments:

- If h^0 is the 126 GeV resonance, $\gamma\gamma$ channel is closely correlated with WW/ZZ. A moderate excess in $\gamma\gamma$ should be accompanied by a corresponding excess in WW/ZZ.

- Combination of theoretical constraints requires $\tan\beta \lesssim 4$. Therefore, the bottom-loop enhancement to the gluon fusion [6] is never a major factor. Regions of $\sin(\beta-\alpha)$ and

$\tan\beta$ are highly restricted once we require the light CP-even Higgs to be the observed 126 GeV scalar particle: $\tan\beta$ between 0.5 to 4 for $\sin(\beta-\alpha)=\pm1$, $\tan\beta$ between 1.5 to 4 for $0.6<\sin(\beta-\alpha)<1$, or the extended region in $\sin(\beta-\alpha)$ with $\tan\beta<1$. The masses of the other Higgses, m_H, m_A, and $m_{H^\pm}$, however, are largely unrestricted and uncorrelated, except for the region where $\sin(\beta-\alpha)>0$ and $m_{A,H^\pm}\gtrsim 600$ GeV, which exhibits a strong correlation between these two masses.

- The discovery of any one of the extra scalars can largely narrow down the parameter space, in particular, if the masses of those particles are relatively high.

- Flavor bounds significantly shrink the allowed parameter space: $\sin(\beta-\alpha)=\pm1$ or $0.6\lesssim\sin(\beta-\alpha)\lesssim 1$. The charged Higgs mass is constrained to lie above 300 GeV.

V. HEAVY HIGGS AT 126 GEV

A. Cross sections and Correlations

It is possible that the 126 GeV resonance discovered at the LHC corresponds to the heavier of the two CP-even Higgses, H^0. There are a few noticeable changes for the heavy H^0 being the SM-like Higgs boson. First of all, since the coupling of the heavy Higgs to a gauge boson pair is scaled by a factor of $\cos(\beta-\alpha)$ as opposed to $\sin(\beta-\alpha)$, demanding SM-like cross sections for H^0 forces us to consider $\sin(\beta-\alpha)\sim 0$, as opposed to $\sin(\beta-\alpha)\sim\pm1$ in the h^0-126 case. Secondly, as will be demonstrated below, the bottom contribution to the gluon fusion production could be significantly enhanced since the range of $\tan\beta$ could be much larger compared to the h^0-126 case.

Similar to Eqs. (14) and (15) as in Sec. IV, the ratios of the gluon fusion cross sections normalized to the SM can be written approximately as:

$$\frac{\sigma(gg\to H^0)}{\sigma_{\rm SM}}=\frac{\sin^2\alpha}{\sin^2\beta}+\frac{\cos^2\alpha}{\cos^2\beta}\frac{|A_{1/2}(\tau_b)|^2}{|A_{1/2}(\tau_t)|^2} \tag{17}$$

$$=\left[\frac{\sin(\beta-\alpha)}{\tan\beta}-\cos(\beta-\alpha)\right]^2+\left[\sin(\beta-\alpha)\tan\beta+\cos(\beta-\alpha)\right]^2\frac{|A_{1/2}(\tau_b)|^2}{|A_{1/2}(\tau_t)|^2}. \tag{18}$$

Contours of $\sigma/\sigma_{\rm SM}(gg\to H^0)=0.5$(green), 1 (red), and 2 (blue) are shown in the left panel of Fig. 10. H^0 couples exactly like the SM Higgs for $\sin(\beta-\alpha)=0$, while deviations from the SM values occur for $\sin(\beta-\alpha)$ away from zero. For $\sin(\beta-\alpha)<0$, $\sigma/\sigma_{\rm SM}(gg\to H^0)$

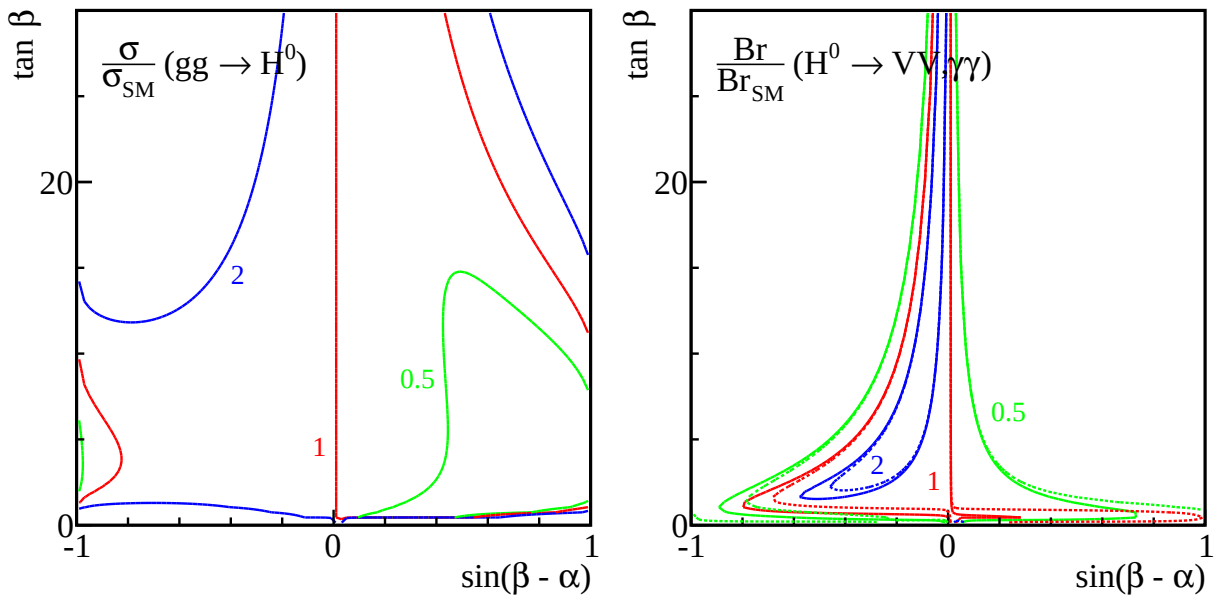

FIG. 10: The normalized $gg \to H^0$ production cross section contours (left panel) and $H^0 \to VV$ (solid lines of the right panel) and $H^0 \to \gamma\gamma$ (dashed lines of the right panel) branching fractions in the H^0-126 case. The contour lines are $\sigma/\sigma_{\rm SM}$, $\mathrm{Br}/\mathrm{Br}_{\rm SM} = 0.5$ (green), 1 (red), and 2 (blue).

is almost always larger than 1 (except for a small region around $\sin(\beta-\alpha) \sim -1$ and $\tan\beta \lesssim 5$), while a suppression of the gluon fusion production is possible for positive values of $\sin(\beta-\alpha)$. This is due to cancellations between the $\sin(\beta-\alpha)$ and $\cos(\beta-\alpha)$ terms in the top Yukawa coupling, in particular, for low $\tan\beta$. The bottom loop contributes significantly when $\tan\beta$ is large, which enhances the gluon fusion production cross section.

$\mathrm{Br}(H^0 \to VV, \gamma\gamma)/\mathrm{Br}_{\rm SM}$ can also be expressed similar to Eq. (16):

$$\frac{\mathrm{BR}(H^0 \to XX)}{\mathrm{BR}(h_{\rm SM} \to XX)} = \frac{\Gamma_{XX}}{\Gamma_{total}} \times \frac{\Gamma^{\rm SM}_{total}}{\Gamma^{\rm SM}_{XX}} = \begin{cases} \frac{\cos^2(\beta-\alpha)}{\cos^2(\beta-\alpha)\mathrm{Br}(h_{\rm SM}\to VV)+\frac{\cos^2\alpha}{\cos^2\beta}\mathrm{Br}(h_{\rm SM}\to bb)+\ldots} \\ \frac{\Gamma(H^0\to\gamma\gamma)/\Gamma(h_{\rm SM}\to\gamma\gamma)}{\cos^2(\beta-\alpha)\mathrm{Br}(h_{\rm SM}\to VV)+\frac{\cos^2\alpha}{\cos^2\beta}\mathrm{Br}(h_{\rm SM}\to bb)+\ldots} \end{cases}, \qquad (19)$$

with the contour lines given in the right panel of Fig. 10. A relative enhancement of the branching fractions over the SM values are observed in extended region of negative $\sin(\beta-\alpha)$, while it is mostly suppressed for positive $\sin(\beta-\alpha)$.

Combining the production cross sections and the decay branching fractions, contours of $gg \to H^0 \to XX$ are given in Fig. 11 for $\gamma\gamma$ (left panel) and WW/ZZ channels (right panel). Requiring the cross section to be consistent with the observed Higgs signal: $0.9 - 2.2$ for the $\gamma\gamma$ channel and $0.2 - 1.4$ for the WW/ZZ channel, results in two distinct regions: a

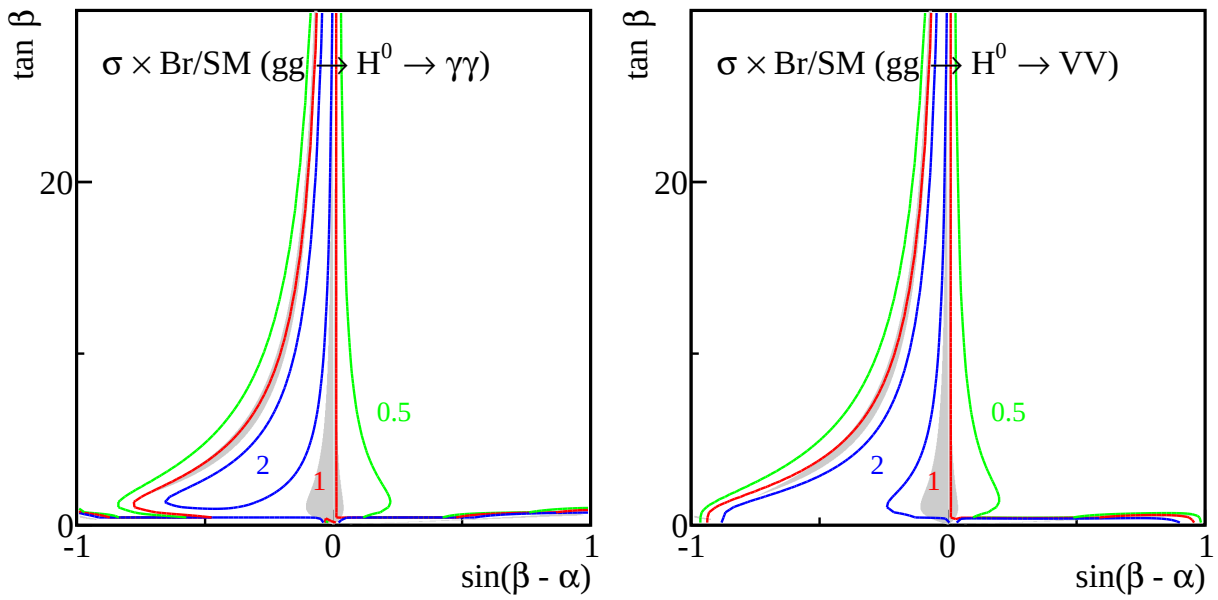

FIG. 11: $\sigma \times \mathrm{Br/SM}$ for the processes $gg \to H^0 \to \gamma\gamma$ (left), and $gg \to H^0 \to WW/ZZ$ (right) in the H^0-126 case. The contour lines are $\sigma \times \mathrm{Br/SM} = 0.5$ (green), 1 (red), and 2 (blue). The shaded gray regions correspond to ones with cross sections of $\gamma\gamma$ and WW/ZZ channels satisfy Eq. (12).

region close to $\sin(\beta - \alpha) \sim 0$, and an extended region of $-0.6 \lesssim \sin(\beta - \alpha) \lesssim -0.1$.

Fig. 12 shows the correlation between the $\gamma\gamma$ and VV channels. Most of the points falls into the diagonal region: $\gamma\gamma : VV \sim 1$. The 95% C.L. exclusion limits from current Higgs searches of WW and ZZ channel limits $\sigma \times \mathrm{Br/SM} < 1.4$ for $\gamma\gamma$ channel as well. A second branch of $\gamma\gamma : WW \sim 2$ also appears, which corresponds to the very low $\tan\beta < 1$ region in Fig. 11. This region is strongly constrained by the flavor bounds, and is therefore not considered further in our study.

B. Parameter Spaces

We now present the results for H^0-126 case with the full parameter scan, including all the theoretical and experimental constraints. Fig. 13 presents the parameter regions in $\tan\beta$ versus $\sin(\beta - \alpha)$. The color coding is the same as in Fig. 4, except that the signal regions in dark red are those with the heavy CP-even Higgs H^0 interpreted as the observed 126 GeV scalar.

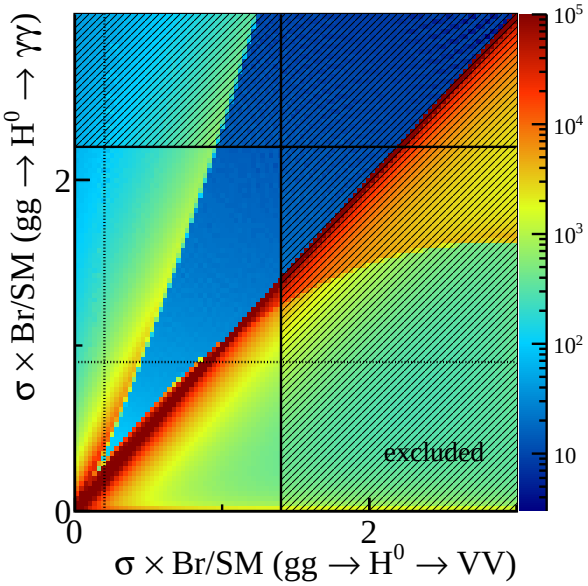

FIG. 12: $\sigma \times \mathrm{Br/SM}$ for $gg \to H^0 \to \gamma\gamma$ versus $gg \to H^0 \to VV$ in the H^0-126 case. Color coding is the same as in Fig. 3.

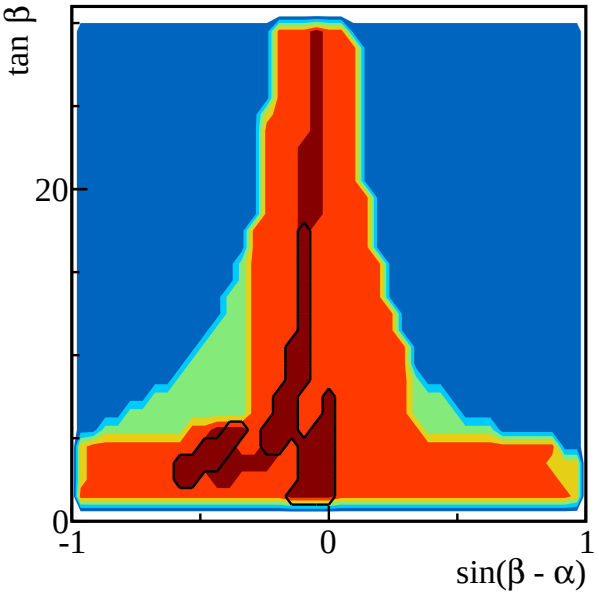

FIG. 13: Parameter regions in the H^0-126 case for $\tan\beta$ versus $\sin(\beta - \alpha)$. Color coding is the same as Fig. 4 except that the dark red regions are the ones consistent with the heavy CP-even Higgs interpreted as the observed Higgs signal.

Requiring the heavy CP-even Higgs to satisfy the cross section ranges of the observed Higgs signal results in two signal regions: one region near $\sin(\beta-\alpha)\sim 0$ and an extended region of $-0.6 \lesssim \sin(\beta-\alpha) \lesssim -0.1$, consistent with Fig. 11. Note however that the region around $\sin(\beta-\alpha)\sim 0$ is actually reduced to $\tan\beta \lesssim 7$. This is because larger values of $\tan\beta$ leads to smaller m_h such that $m_h < m_H/2$ (see right panel of Fig. 14 below). The opening of $H^0 \to h^0 h^0$ channel reduces the the branching fractions of $H^0 \to WW/ZZ, \gamma\gamma$ to be outside the signal cross section region. Regions surviving the flavor bounds are the ones enclosed by black curves. Larger values of $\tan\beta \gtrsim 17$ are disfavored.

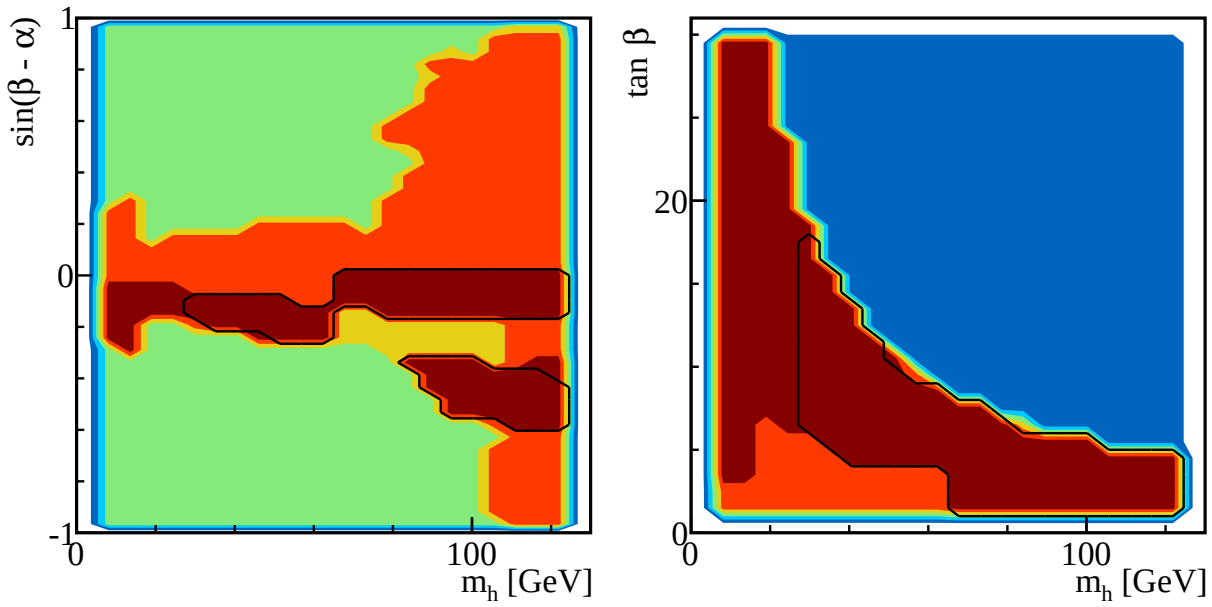

FIG. 14: Parameter regions in the H^0-126 case for $\sin(\beta-\alpha)$ versus m_h (left panel) and $\tan\beta$ versus m_h (right panel). Color coding is the same as Fig. 13.

Fig. 14 shows the parameter region in $\sin(\beta-\alpha)$ versus m_h (left panel) and $\tan\beta$ versus m_h (right panel). Within the narrow region around $\sin(\beta-\alpha)\sim 0$, m_h can take all values up to 126 GeV. For $-0.6 \lesssim \sin(\beta-\alpha) \lesssim -0.4$, when the H^0WW, H^0ZZ couplings could significantly deviate from the SM value while h^0WW, h^0ZZ couplings are sizable, the light CP-even Higgs mass is constrained to be larger than about 80 GeV from LEP Higgs searches [33, 34]. This is the interesting region where the two Higgses are close to being degenerate, with both h^0 and H^0 showing significant deviation of their couplings to gauge bosons from the SM value.

The right panel of Fig. 14 shows the parameter region of $\tan\beta$ versus m_h. Larger values

of $\tan\beta$ is only allowed for small values of m_h. The red region where $m_h < 60$ GeV and $\tan\beta \lesssim 5$ can not satisfy the Higgs signal cross section requirement due to the opening of $H^0 \to h^0 h^0$ mode, which corresponds to the $m_h < 60$ GeV, $\sin(\beta-\alpha) \sim 0$ red region in the $\sin(\beta-\alpha)$ versus m_h plot (left panel of Fig. 14). Imposing the flavor bounds further rules out regions with light m_h below about 25 GeV, mainly due to the process $B_s \to \mu^+\mu^-$. Large values of $\tan\beta \gtrsim 17$ are excluded correspondingly.

Fig. 15 shows $\sin(\beta-\alpha)$ versus $m_{A,H^\pm}$ (left panels) and $\tan\beta$ versus $m_{A,H^\pm}$ (right panels). The plots for m_A and $m_{H^\pm}$ are very similar, except for very low masses. Very large values of $m_{A,H^\pm} \gtrsim 800$ GeV are excluded by theoretical considerations, similar to the h^0-126 case. $m_A \lesssim 80$ GeV and $\tan\beta \gtrsim 5$ are excluded by the LEP Higgs search [33], while the triangle region of $130 \lesssim m_A \lesssim 250$ GeV and $\tan\beta \gtrsim 13$ is excluded by the LHC searches for the CP-odd Higgs in $\tau\tau$ mode [38, 39]. For the charged Higgs, small values of $m_{H^\pm} \lesssim 80$ GeV are ruled out by LEP searches on charged Higgs [35, 36]. Tevatron and the LHC charged Higgs searches [38, 39]: $t \to H^\pm b \to \tau\nu_\tau b$ further rule out regions of $m_{H^\pm} \lesssim 150$ GeV and $\tan\beta \gtrsim 17$. The small triangle in $m_{H^\pm}$ versus $\tan\beta$ plot for 200 GeV $\lesssim m_{H^\pm} \lesssim 300$ GeV and $\tan\beta \gtrsim 25$ is translated from the corresponding region in $\tan\beta$ versus m_A, due to the correlation between m_A and $m_{H^\pm}$ introduced by $\Delta\rho$, as shown below in Fig. 16. Imposing the flavor constraints further limits $m_A \gtrsim 250$ GeV, $m_{H^\pm} \gtrsim 300$ GeV and $\tan\beta \lesssim 17$.

m_A and $m_{H^\pm}$ exhibit a much stronger correlation in the H^0-126 case, mostly due to the the $\Delta\rho$ constraints, as shown in the left panel of Fig. 16. Comparing with the h^0-126 case, in which m_H could be large with a relaxed constraints on m_A and $m_{H^\pm}$ mass correlation, in the H^0-126 case, both m_h and m_H are relatively small. m_A and $m_{H^\pm}$ should therefore be highly correlated in order to avoid large custodial symmetry breaking in the Higgs sector. However, there is a small strip of allowed region at $m_{H^\pm} \sim 100$ GeV with m_A between $150 - 700$ GeV. This region escapes the $\Delta\rho$ constraint since for $m_{H^\pm} \sim m_h \sim m_H$, the contribution to $\Delta\rho$ introduced by the large mass difference between m_A and $m_{H^\pm}$ is cancelled by the $(h^0,\ A^0)$ loop and $(H^0,\ A^0)$ loop. Imposing the flavor constraints again limits $m_{H^\pm}$ to be larger than 300 GeV. m_A is constrained to be more than 250 GeV as well due to the correlations.

The right panel of Fig. 16 shows the parameter region of m_A versus m_h, which does not show much correlation. For $m_h \lesssim 90$ GeV, low values of $m_A \lesssim 100$ GeV is excluded by LEP searches of $h^0 A^0$ channel [33]. High values of $m_A \gtrsim 600$ GeV are excluded for $m_h < 90$ GeV. This is because such a large value of m_A can only be realized for $|\sin(\beta-\alpha)| > 0.3$ (see

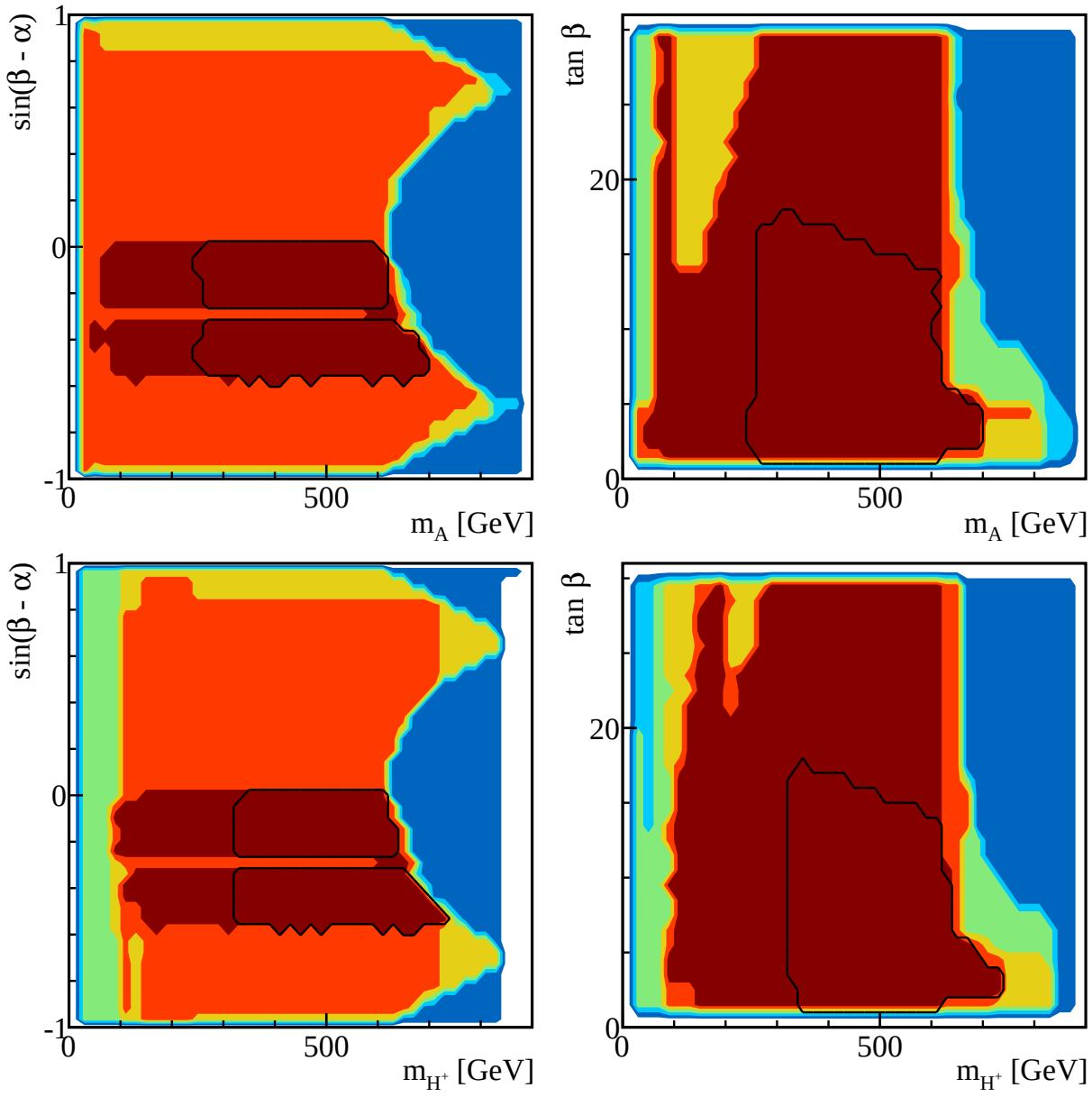

FIG. 15: Parameter regions in the H^0-126 case for $\sin(\beta-\alpha)$ versus m_A (upper left panel) and $\tan\beta$ versus m_A (upper right panel), as well as similar plots for $m_H^{\pm}$ (lower panels). Color coding is the same as Fig. 13.

the upper-left panel of Fig. 15). Such regions of $|\sin(\beta-\alpha)| > 0.3$ and $m_h < 90$ GeV are excluded by the LEP Higgs search of $h^0 Z$ channel [34], as shown clearly in the m_h versus $\sin(\beta-\alpha)$ plot (left panel of Fig. 14). Such excluded regions for large m_A (and large $m_{H^\pm}$ due to correlation) also appears in the $\tan\beta$ versus m_A ($m_{H^\pm}$) plots in Fig. 15.

We end the section with the following observations:

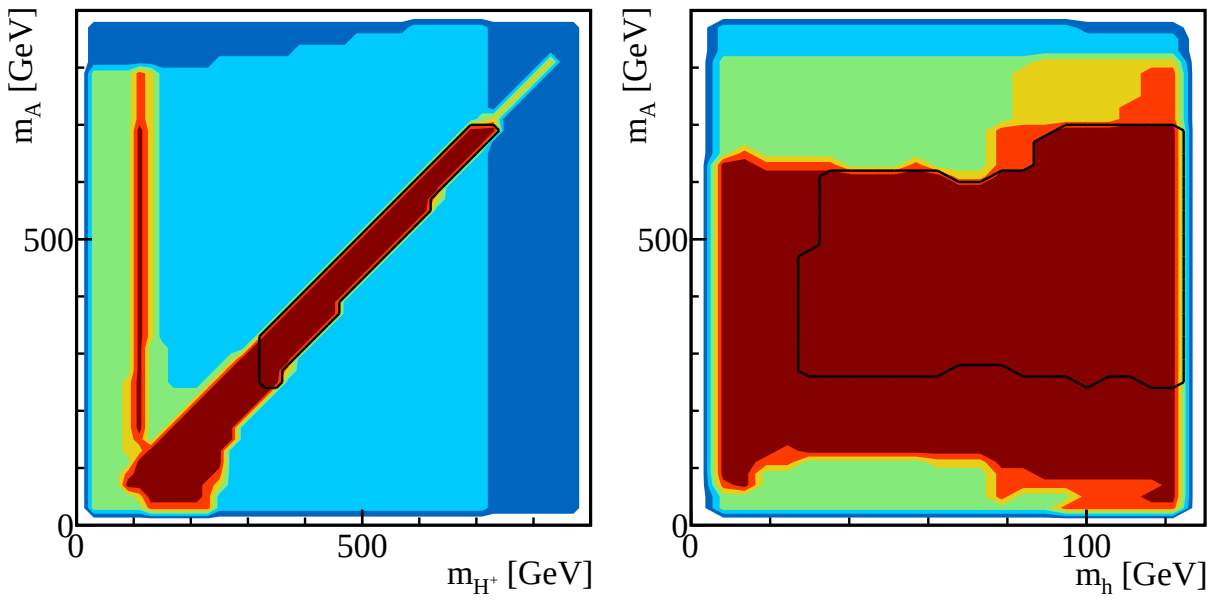

FIG. 16: Parameter regions in the H^0-126 case for m_A versus $m_{H^\pm}$ (left panel) and m_h (right panel). Color coding is the same as Fig. 13.

- Contrary to the h^0-126 case, fixing the heavy CP-even Higgses to be the 126 GeV resonance forces us into a small narrow region of $\sin(\alpha-\beta)\sim 0$ with $\tan\beta \lesssim 7$ or an extended region of $-0.6 \lesssim \sin(\alpha-\beta) \lesssim -0.1$ with far less restricted value of $\tan\beta$.

- The light CP-even Higgs can have mass of any value up to 126 GeV, with smaller m_h only allowed for $\sin(\beta-\alpha)\sim 0$. Note that the case of nearly degenerate h^0 and H^0 is allowed, as studied in detail in Ref. [19].

- m_A and $m_{H^\pm}$ exhibit strong correlations: $m_A \simeq m_{H^\pm}$, due to $\Delta\rho$ constraints.

- Flavor bounds impose the strong constraint: $\tan\beta \lesssim 17$, $m_h > 20$ GeV, and $m_{H^\pm} >$300 GeV. m_A is also constrained to be more than 250 GeV due to the correlation between m_A and $m_{H^\pm}$.

VI. OTHER HIGGS CHANNELS

Thus far, we have concentrated on the gluon fusion production mechanism and the dominant $\gamma\gamma$, ZZ and WW decay channels for the Higgs. The vector boson fusion channel is another important production channel for the CP-even Higgses. For certain Higgs decay

channels, for example, $\tau\tau$ mode, VBF production is the one that provides the dominant sensitivity due to the excellent discrimination of the backgrounds using the two forward tagging jets and the central jet-veto [45]. Other production channels, VH and ttH associated production, can also be of interest for Higgs decay to bb. In this section, we discuss the cross sections in other search channels for both h^0 and H^0 when they are interpreted as the observed 126 GeV scalar.

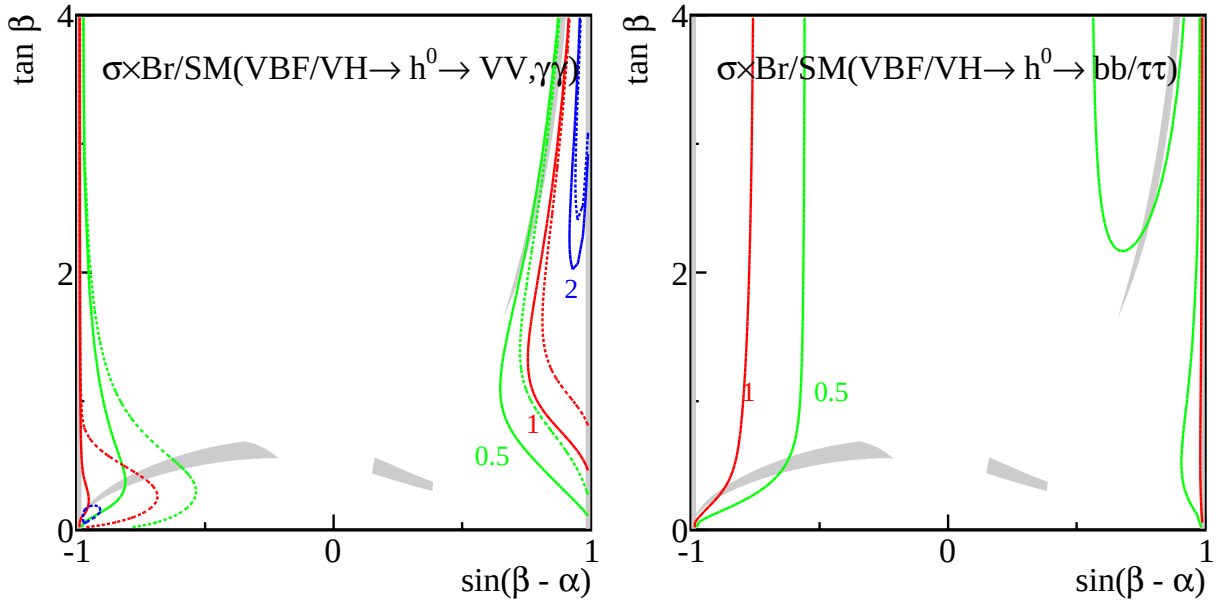

FIG. 17: $\sigma \times$ Br/SM for $VBF/VH \to h^0 \to WW/ZZ$ (solid curves in left panel), $\gamma\gamma$ (dashed curves in left panel) and $VBF/VH \to h^0 \to bb/\tau\tau$ (right panel) for the h^0-126 case. The contour lines show $\sigma \times$ Br/SM = 0.5(green), 1 (red) and 2 (blue). The shaded gray regions correspond to ones with cross sections of $\gamma\gamma$ and WW/ZZ channels satisfy Eq. (12).

In Fig. 17, we show the normalized cross sections for the WW/ZZ, $\gamma\gamma$ (left panel) and $bb/\tau\tau$ (right panel) final states via VBF or VH associated production (both production cross sections are controlled by h^0VV coupling) in the $\tan\beta$ versus $\sin(\beta-\alpha)$ plane for the h^0-126 case. For $VBF/VH \to h^0 \to WW/ZZ$, both the production and decay are proportional to $\sin(\beta-\alpha)$, resulting in regions highly centered around $\sin(\beta-\alpha) \sim \pm 1$ for any enhancement above the SM value. For the currently preferred gray Higgs signal regions near $\sin(\beta-\alpha) \sim \pm 1$, $VBF/VH \to h^0 \to WW/ZZ$ is typically in the range of $0.5 - 1$ of the SM value, while a strong suppression of 0.1 could occur in the extended $\sin(\beta-\alpha)$ signal regions with small $\tan\beta < 1$.

For $VBF/VH \to h^0 \to bb/\tau\tau$, the cross section is suppressed for most of the regions, except in the neighborhood of $\sin(\beta-\alpha) = \pm 1$ where SM rates can be achieved. The current preferred signal regions typically have a suppression of 0.5 or stronger for this $bb/\tau\tau$ channel. There is also a strong inverse correlation between the WW/ZZ and $bb/\tau\tau$ channels, since an increase in bb decay branching fraction can only occur at the expense of WW.

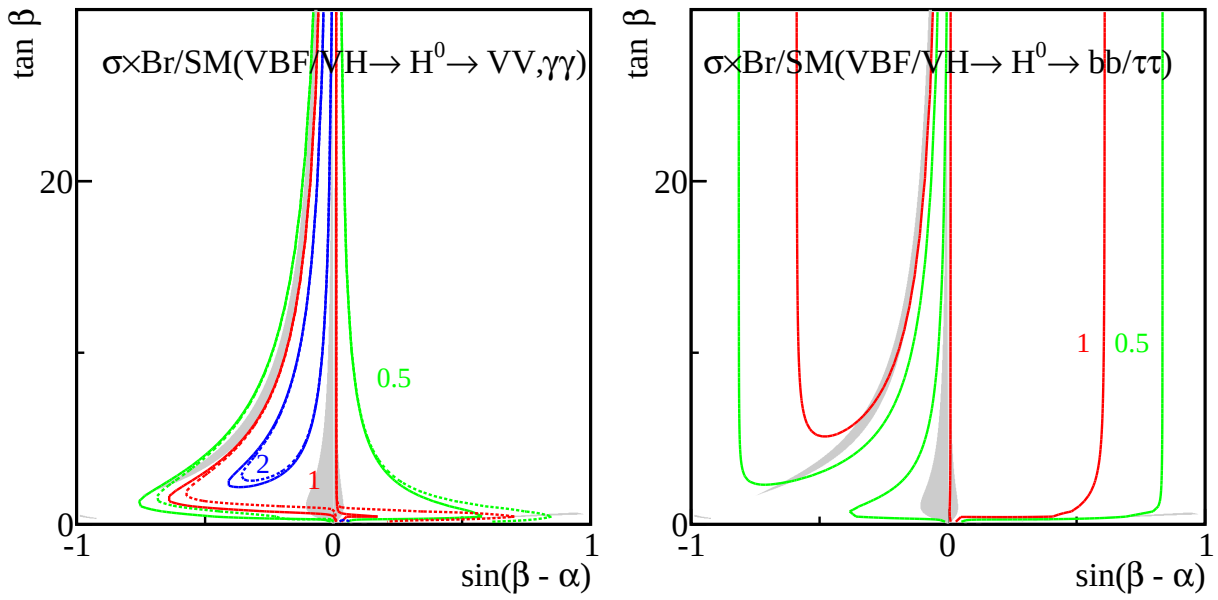

FIG. 18: $\sigma \times$ Br/SM for $VBF/VH \to H^0 \to WW/ZZ, \gamma\gamma$ (left) and $VBF/VH \to H^0 \to bb/\tau\tau$ (right) for the H^0-126 case. Color coding is the same as in Fig. 17.

Fig. 18 show the $\sigma \times$Br/SM plots for VV, $\gamma\gamma$, and $bb/\tau\tau$ channel via VBF/VH production for the H^0-126 case. The qualitative features of the VV, $\gamma\gamma$ plot is the same as that of Fig. 11. The currently favored gray signal regions typically correspond to a normalized cross section of $VBF/VH \to H^0 \to WW/ZZ$ around 1 as well.

The $bb/\tau\tau$ channel, however, exhibits a very different behavior. For two regions of $-0.6 \leq \sin(\beta-\alpha) \leq -0.1$ and $0 \leq \sin(\beta-\alpha) \leq 0.6$ (regions enclosed by the red curves in the right panel of Fig. 18), a normalized cross section of at least the SM signal strength can be achieved. A strong suppression, sometime as small as 0.1, can be obtained in the other regions. The currently favored gray signal region near $\sin(\beta-\alpha) \sim 0$ corresponds to $\sigma/\sigma_{\rm SM}$ of order 1 for $VBF/VH \to H^0 \to bb/\tau\tau$ channel, while a suppression as large as 0.5 is possible for the extended regions in negative $\sin(\beta-\alpha)$. The inverse correlation between $bb/\tau\tau$ and WW channels also appears in the H^0-126 case.

We also studied $gg \to h^0, H^0 \to bb/\tau\tau$ channel for both the h^0-126 and H^0-126 cases, and noticed that for the currently favored higgs signal regions, a factor of 2 enhancement could be realized.

VII. CONCLUSIONS

In this paper, we presented a detailed analysis of the Type II 2HDM (with an imposed Z_2 symmetry) parameter space, identifying either the light or the heavy CP-even Higgs as the recently discovered resonance at 126 GeV. We scanned the remaining five parameters $\sin(\beta-\alpha)$, $\tan\beta$, m_A, $m_{H^\pm}$, and m_H or m_h while fixing either m_h or m_H to be 126 GeV. We took into account all the theoretical constraints as well as current experimental search limits on the Higgses. We further studied the implications on the parameter space once flavor constraints are imposed. We found unique features in each of these two cases.

In the h^0-126 case, we are forced into regions of parameter space where $\sin(\beta-\alpha) \sim \pm 1$, and $\tan\beta$ is not too large ($\lesssim 4$), or extended regions of $-1 \lesssim \sin(\beta-\alpha) \lesssim -0.2$, $0.2 \lesssim \sin(\beta-\alpha) \lesssim 0.4$ with $\tan\beta < 1$. There is, however, a wide range of values that are still allowed for the masses of the heavy CP-even, pseudo scalar and charged Higgses. The Higgs masses are typically not correlated, except in the region where $\sin(\beta-\alpha) > 0$ and $m_{A,H^\pm} \gtrsim 600$ GeV, which exhibit a strong correlation between m_A and $m_{H^\pm}$ because of the $\Delta\rho$ constraint. Imposing flavor constraints further restricts $\sin(\beta-\alpha)$ to be near -1 or between 0.6 to 1, and $m_{H^\pm} > 300$ GeV.

In the H^0-126 case, we are forced into an orthogonal region of parameter space where $\sin(\beta-\alpha) \sim 0$, $\tan\beta \lesssim 7$ or an extended region of $-0.6 \lesssim \sin(\alpha-\beta) \lesssim -0.1$ with less restricted $\tan\beta$. m_A and $m_{H^\pm}$ exhibit strong correlations: $m_A \simeq m_{H^\pm}$, due to the $\Delta\rho$ constraint. The interesting scenario of the light CP-even Higgs being close to 126 GeV still survives. Imposing flavor bounds further shrinks the parameter space considerably: $\tan\beta \lesssim 17$, $m_h > 20$ GeV, $m_{H^\pm} >$300 GeV, and $m_A > 250$ GeV.

We find that in either of these scenarios, one can identify regions of parameter space that pass all theoretical and experimental bounds and still allow a slightly higher than SM rate to diphotons. $\gamma\gamma$ and WW/ZZ rates are most likely strongly correlated: $\gamma\gamma : VV \sim 1$ for the normalized cross sections. It is possible, though much less likely, that for h^0-126 case with negative $\sin(\beta-\alpha)$, a factor of two enhancement of $\gamma\gamma$ rate can occur, accompanied

by the WW/ZZ rate around the SM value.

We further studied the implication for the Higgs production via VBF or VH process, and decays to bb, $\tau\tau$ channels. We found that in the h^0-126 case, both $VBF/VH \to h^0 \to bb/\tau\tau, WW/ZZ$ could be significantly suppressed in the Higgs signal region. For the H^0-126 case, $VBF/VH \to H^0 \to WW/ZZ$ channel is almost the SM strength. Possible suppression of $bb/\tau\tau$ channel up to 0.5 is possible for the extended signal regions in negative $\sin(\beta-\alpha)$. Future observation of the bb and $\tau\tau$ modes can provide valuable information for the parameter regions of the type II 2HDM.

Comparing to the Minimal Supersymmetric Standard Model, with its Higgs sector being a restricted type II 2HDM and the tree level Higgs spectrum completely determined by m_A and $\tan\beta$, the parameter regions of the general Type II 2HDM is much more relaxed. Unlike the MSSM in which the h^0-126 case corresponds to the decoupling region of $m_A \gtrsim 300$ GeV, and the H^0-126 GeV case corresponds to the non-decoupling region of $m_A \sim 100-130$ GeV [46], the value of m_A in the general Type II 2HDM could vary over the entire viable region up to about 800 GeV. The MSSM relation of $m_A \sim m_{H^\pm} \sim m_H$ in the decoupling region is also much more relaxed in the Type II 2HDM. No obvious correlation is observed between m_A, $m_{H^\pm}$, and m_H for the h^0-126 case, except for the region with large $m_{A,H^\pm} \gtrsim 600$ GeV.

Observations of extra Higgses in the future would further pin down the Higgs sector beyond the SM. While the conventional decay channels of Higgses to SM particles continue to be important channels to search for extra Higgses, novel decay channels of a heavy Higgs into light Higgses or light Higgs plus gauge boson could also appear. Future work along the lines of collider phenomenology of multiple Higgs scenarios is definitely warranted.

Acknowledgments

We thank L. Carpenter for her participation at the beginning of this project. We would also like to thank David Lopez-Val for useful discussions and Oscar Stål for sharing the 2HDMC package. This work was supported by the Department of Energy under Grant DE-FG02-04ER-41298.

[1] G. Aad *et al.* [ATLAS Collaboration], Phys. Lett. B **716**, 1 (2012) [arXiv:1207.7214 [hep-ex]].

[2] **ATLAS** Collaboration, G. Aad et al., *Combined measurements of the mass and signal strength of the Higgs-like boson with the ATLAS detector using up to 25* fb^{-1} *of proton-proton collision data*, Tech. Rep. ATLAS-CONF-2013-014.

[3] S. Chatrchyan *et al.* [CMS Collaboration], Phys. Lett. B **716**, 30 (2012) [arXiv:1207.7235 [hep-ex]].

[4] **CMS** Collaboration, S. Chatrchyan et al., *Combination of standard model Higgs boson searches and measurements of the properties of the new boson with a mass near 125 GeV*, Tech. Rep. CMS-PAS-HIG-13-005.

[5] **ATLAS** Collaboration, G. Aad et al., *Study of the spin of the new boson with up to 25* fb^{-1} *of ATLAS data*, Tech. Rep. ATLAS-CONF-2013-040; *Combined coupling measurements of the Higgs-like boson with the ATLAS detector using up to 25* fb^{-1} *of proton-proton collision data*, Tech. Rep. ATLAS-CONF-2013-034.

[6] G. C. Branco, P. M. Ferreira, L. Lavoura, M. N. Rebelo, M. Sher and J. P. Silva, Phys. Rept. **516**, 1 (2012) [arXiv:1106.0034 [hep-ph]].

[7] H.E. Haber, G.L. Kane and T. Sterling, Nucl. Phys. **B161**, 493 (1979).

[8] L.J. Hall and M.B. Wise, Nucl. Phys. **B187**, 397 (1981).

[9] J.F. Donoghue and L.F. Li, Phys. Rev. **D19**, 945 (1979).

[10] P. M. Ferreira, R. Santos, M. Sher and J. P. Silva, Phys. Rev. D **85**, 077703 (2012) [arXiv:1112.3277 [hep-ph]].

[11] P. M. Ferreira, R. Santos, M. Sher and J. P. Silva, Phys. Rev. D **85**, 035020 (2012) [arXiv:1201.0019 [hep-ph]].

[12] H. S. Cheon and S. K. Kang, arXiv:1207.1083 [hep-ph].

[13] A. Drozd, B. Grzadkowski, J. F. Gunion and Y. Jiang, arXiv:1211.3580 [hep-ph].

[14] S. Chang, S. K. Kang, J. -P. Lee, K. Y. Lee, S. C. Park and J. Song, arXiv:1210.3439 [hep-ph].

[15] C. -Y. Chen and S. Dawson, arXiv:1301.0309 [hep-ph].

[16] B. Grinstein and P. Uttayarat, arXiv:1304.0028 [hep-ph].

[17] N. Craig and S. Thomas, JHEP **1211**, 083 (2012) [arXiv:1207.4835 [hep-ph]].

[18] L. Basso, A. Lipniacka, F. Mahmoudi, S. Moretti, P. Osland, G. M. Pruna and M. Purmohammadi, JHEP **1211**, 011 (2012) [arXiv:1205.6569 [hep-ph]].

[19] P. M. Ferreira, H. E. Haber, R. Santos and J. P. Silva, arXiv:1211.3131 [hep-ph].

[20] G. Burdman, C. E. F. Haluch and R. D. Matheus, Phys. Rev. D **85**, 095016 (2012)

[arXiv:1112.3961 [hep-ph]].

[21] B. Coleppa, K. Kumar and H. E. Logan, Phys. Rev. D **86**, 075022 (2012) [arXiv:1208.2692 [hep-ph]].

[22] S. Davidson and H. E. Haber, Phys. Rev. D **72**, 035004 (2005) [Erratum-ibid. D **72**, 099902 (2005)] [hep-ph/0504050]; H. E. Haber and D. O'Neil, Phys. Rev. D **74**, 015018 (2006) [hep-ph/0602242].

[23] D. Eriksson, J. Rathsman and O. Stal, Comput. Phys. Commun. **181**, 189 (2010) [arXiv:0902.0851 [hep-ph]].

[24] P. Bechtle, O. Brein, S. Heinemeyer, G. Weiglein and K. Williams, AIP Conf. Proc. **1200**, 510 (2010) [arXiv:0909.4664 [hep-ph]].

[25] P. Bechtle, O. Brein, S. Heinemeyer, G. Weiglein and K. E. Williams, PoS CHARGED **2010**, 027 (2010) [arXiv:1012.5170 [hep-ph]].

[26] P. Bechtle, O. Brein, S. Heinemeyer, G. Weiglein and K. E. Williams, Comput. Phys. Commun. **182**, 2605 (2011) [arXiv:1102.1898 [hep-ph]].

[27] N. G. Deshpande and E. Ma, Phys. Rev. D **18**, 2574 (1978); M. Sher, Phys. Rept. **179**, 273 (1989); A. W. El Kaffas, W. Khater, O. M. Ogreid and P. Osland, Nucl. Phys. B **775**, 45 (2007) [hep-ph/0605142].

[28] I. F. Ginzburg and I. P. Ivanov, Phys. Rev. D **72**, 115010 (2005) [hep-ph/0508020].

[29] K. Nakamura *et al.* [Particle Data Group Collaboration], J. Phys. G **37**, 075021 (2010).

[30] J. F. Gunion, H. E. Haber, G. Kane, S. Dawson, *The Higgs Hunter's Guide*, Addison-Wesley Publishing Company, 1990.

[31] **ATLAS** Collaboration, G. Aad et al., *Measurements of the properties of the Higgs-like boson in the $WW(*) \to l\nu l\nu$ decay channel with the ATLAS detector using 25* fb^{-1} *of proton-proton collision data*, Tech. Rep. ATLAS-CONF-2013-030; *Measurements of the properties of the Higgs-like boson in the two photon decay channel with the ATLAS detector using 25* fb^{-1} *of proton-proton collision data*, Tech. Rep. ATLAS-CONF-2013-012; *Measurements of the properties of the Higgs-like boson in the four lepton decay channel with the ATLAS detector using 25* fb^{-1} *of proton-proton collision data*, Tech. Rep. ATLAS-CONF-2013-013; *Search for the Standard Model Higgs boson produced in association with top quarks in proton-proton collisions at* $\sqrt{s} = 7$TeV *using the ATLAS detector*, Tech. Rep. ATLAS-CONF-2012-135; Phys. Lett. B **718**, 369 (2012) [arXiv:1207.0210 [hep-ex]]; JHEP **1209**, 070 (2012) [arXiv:1206.5971

[hep-ex]].

[32] **CMS** Collaboration, S. Chatrchyan et al., *Updated measurements of the Higgs boson at 125 GeV in the two photon decay channel*, Tech. Rep. CMS-PAS-HIG-13-001; *Properties of the Higgs-like boson in the decay H to ZZ to 4l in pp collisions at sqrt s =7 and 8 TeV*, Tech. Rep. CMS-PAS-HIG-13-002; *Evidence for a particle decaying to W+W- in the fully leptonic final state in a standard model Higgs boson search in pp collisions at the LHC* , Tech. Rep. CMS-PAS-HIG-13-003; *Search for the Standard-Model Higgs boson decaying to tau pairs in proton-proton collisions at sqrt(s) = 7 and 8 TeV* , Tech. Rep. CMS-PAS-HIG-13-004; *Search for Higgs boson production in association with top quark pairs in pp collisions*, Tech. Rep. CMS-PAS-HIG-12-025; *Search for the standard model Higgs boson produced in association with W or Z bosons, and decaying to bottom quarks for HCP 2012*, Tech. Rep. CMS-PAS-HIG-12-044.

[33] **ALEPH** Collaboration, **DELPHI** Collaboration, **L3** Collaboration, **OPAL** Collaboration, **LEP Working Group** for Higgs Boson Searches Collaboration, S. Schael et al., *Search for neutral MSSM Higgs bosons at LEP*, *Eur.Phys.J.* **C47** (2006) 547–587, [hep-ex/0602042].

[34] **LEP Working Group** for Higgs boson searches, **ALEPH** Collaboration, **DELPHI** Collaboration, **L3** Collaboration, **OPAL** Collaboration, R. Barate et al., *Search for the standard model Higgs boson at LEP*, *Phys.Lett.* **B565** (2003) 61–75, [hep-ex/0306033].

[35] **LEP Higgs Working Group** for Higgs boson searches, **ALEPH** Collaboration, **DELPHI** Collaboration, **L3** Collaboration, **OPAL** Collaboration, *Search for charged Higgs bosons: Preliminary combined results using LEP data collected at energies up to 209-GeV*, hep-ex/0107031.

[36] **ALEPH** Collaboration, A. Heister et al., *Search for charged Higgs bosons in e^+e^- collisions at energies up to $\sqrt{s}$ = 209-GeV*, *Phys.Lett.* **B543** (2002) 1–13, [hep-ex/0207054].

[37] **Tevatron New Physics Higgs Working Group** and **CDF** and **D0** Collaborations, arXiv:1207.0449 [hep-ex].

[38] **ATLAS** Collaboration, G. Aad et al., *Search for Neutral MSSM Higgs bosons in sqrt(s)=7 TeV pp collisions at ATLAS*, Tech. Rep. ATLAS-CONF-2012-094. JHEP **1206**, 039 (2012) [arXiv:1204.2760 [hep-ex]]; arXiv:1302.3694 [hep-ex].

[39] S. Chatrchyan *et al.* [CMS Collaboration], Phys. Lett. B **713**, 68 (2012) [arXiv:1202.4083 [hep-ex]]; *Higgs to tau tau (MSSM) (HCP)*, Tech. Rep. CMS-PAS-HIG-12-050; arXiv:1302.2892

[hep-ex]; JHEP **1207**, 143 (2012) [arXiv:1205.5736 [hep-ex]].

[40] F. Mahmoudi, Comput. Phys. Commun. **180**, 1579 (2009) [arXiv:0808.3144 [hep-ph]].

[41] Y. Amhis *et al.* [Heavy Flavor Averaging Group Collaboration], arXiv:1207.1158 [hep-ex], and online updates at http://www.slac.stanford.edu/xorg/hfag.

[42] A. G. Akeroyd and F. Mahmoudi, JHEP **0904**, 121 (2009) [arXiv:0902.2393 [hep-ph]].

[43] R. Aaij *et al.* [LHCb Collaboration], Phys. Rev. Lett. **108**, 231801 (2012) [arXiv:1203.4493 [hep-ex]].

[44] F. Mahmoudi and O. Stal, Phys. Rev. D **81**, 035016 (2010) [arXiv:0907.1791 [hep-ph]].

[45] D. L. Rainwater, D. Zeppenfeld and K. Hagiwara, Phys. Rev. D **59**, 014037 (1998) [hep-ph/9808468].

[46] N. D. Christensen, T. Han and S. Su, Phys. Rev. D **85**, 115018 (2012) [arXiv:1203.3207 [hep-ph]].